

Searching for Variability in the Globular Cluster Messier 4¹

Robert D. Ferdman², James Brewer², Greg G. Fahlman³, Brad K. Gibson⁴, Brad M. S. Hansen⁵, Mark E. Huber², Rodrigo A. Ibata⁶, Jasonot S. Kalirai², Jaymie M. Matthews², R. Michael Rich⁵, Harvey B. Richer², Jason F. Rowe², Michael M. Shara⁷, and Peter B. Stetson³

ABSTRACT

Time-series data taken with the *Hubble Space Telescope* of a field six core radii ($\sim 5'$) from the center of the globular cluster Messier 4, and covering a period of about 10 weeks in early 2001, have been analyzed in search of variable objects. Various criteria were employed to select candidate variable stars. Period searches were performed on the selected candidates using phase dispersion minimization (PDM). The reliability of the PDM search results was tested using synthetic light curves of eclipsing binary stars and sinusoidal light curves at different periods. Results from this analysis showed that there are probably no eclipsing binary stars or periodic variables in our field with periods on the order of a few hours to a few days, down to limiting magnitudes of $V \sim 25$ and $I \sim 24$, which is consistent with the absence of contact binaries such as W Ursae Majoris systems. However, one

¹Based on observations with the NASA/ESA *Hubble Space Telescope*, obtained at the Space Telescope Science Institute, which is operated by the Association of Universities for Research in Astronomy, Inc., under NASA contract NAS5-26555. These observations are associated with proposal GO-8679.

²Department of Physics and Astronomy, University of British Columbia, 6224 Agricultural Road, Vancouver, BC V6T 1Z4, Canada; ferdman@astro.ubc.ca, jbrewer@astro.ubc.ca, jkalirai@astro.ubc.ca, richer@astro.ubc.ca, rowe@astro.ubc.ca.

³National Research Council, Herzberg Institute of Astrophysics, 5071 West Saanich Road, RR5, Victoria, BC V9E 2E7, Canada; greg.fahlman@NRC-CNRC.gc.ca, peter.stetson@NRC-CNRC.gc.ca.

⁴Centre for Astrophysics and Supercomputing, Swinburne University, P.O. Box 218, Hawthorn, VIC 3122, Australia; bgibson@astro.swin.edu.au.

⁵Division of Astronomy, University of California at Los Angeles, 405 Hilgard Avenue, Los Angeles, CA 90095; hansen@astro.ucla.edu, rmr@astro.ucla.edu.

⁶Observatoire de Strasbourg, 11 rue de l'Universite, F-67000 Strasbourg, France; ibata@newb6.u-strasbg.fr.

⁷Department of Astrophysics, Division of Physical Sciences, American Museum of Natural History, Central Park West at 79th Street, New York, NY 10024-5192; mshara@amnh.org.

candidate variable star does show an increase in brightness of ~ 0.1 magnitudes in both bandpasses, which seems to last for a few days. Possible explanations concerning the nature of this object include a binary system with a white dwarf primary and a low-mass main sequence secondary, or a BY Draconis variable star. We are able to set an upper limit to the observed binary fraction in this dataset of 0.05%.

Subject headings: binaries: eclipsing—stars: variables—globular clusters: individual (M4)

1. Introduction

It is well known that binary stars are important for the determination of stellar masses. In addition, knowledge of the population of these objects in globular clusters (GCs) is fundamental to understanding the evolution and dynamical history of GCs. Even a small fraction of binary stars in a cluster can contribute greatly in preventing or delaying core collapse of the cluster. A full treatment of this topic can be found in Hut et al. (1992).

This paper presents the results of a search for variability in faint objects in a time-series data set taken with the *Hubble Space Telescope* (*HST*) in a field of the globular cluster M4 (NGC 6121; $\alpha = 16^h 23^m 54\rlap{.}^s 61$, $\delta = 26^\circ 32' 23\rlap{.}'' 93$ (J2000)). Even though the the data were not primarily collected to search for variable stars, the potential for the discovery of such objects did exist, since it included 246 separate observations of the same field over about two and a half months. The images represented the deepest ever imaging of a globular cluster, reaching the faintest part of the white dwarf sequence ever observed. In the context of this project, it allowed for the study of variability within magnitude ranges that have seldom been explored. Another recent study was performed with *HST* by Albrow et al. (2001) in which nearly continuous observations for 8.3 days were taken in the core of the globular cluster 47 Tucanae for the primary purpose of searching for planetary transits. Although no such transits were found, the study did identify 114 variables, most of which are believed to be binary systems.

In the color-magnitude diagrams of globular clusters, observations of a binary star sequence 0.75 magnitudes brighter than the main sequence are rare. Even in cases where one is found, many stars in the sequence are actually optical doubles, due to the effects of crowding in globular cluster images. However, binary stars have been found in globular clusters (see, e.g., Yan and Mateo (1994), Rubenstein and Bailyn (1996), and Kaluzny et al. (1997)). In fact, W UMa type eclipsing binaries are among the most common type of short-period

variable stars found in GCs (Rucinski 2000).

In addition to binary systems, the data were probed for other types of variable objects, such as pulsating stars, planetary transits, as well as nonperiodic objects such as flare stars, and supernovae in background galaxies. The study of these objects is vital to research in diverse areas such as stellar populations, cosmology, and the evolution of stars, clusters, and galaxies.

The following section deals with the observations of M4 and the reduction of the data. Section 3 discusses what one may expect to find in these data based on previous studies of M4, as well as other globular clusters observed with *HST*. Section 4 describes the process of selecting candidate variable stars, and section 5 discusses how these candidates were searched for periodicity. Section 6 explains how the reliability of results obtained from the period searches were tested. Section 7 describes searches for nonperiodic variable stars, and in particular searches for supernovae. Sections 8 and 9 present and discuss results of the analysis. Finally, section 10 provides some concluding remarks.

2. Observations and Data Reduction

The data are taken from *Hubble Space Telescope* (*HST*) observations of M4 in the program GO 8679 (cycle 9), using the Wide Field Planetary Camera 2 (WFPC2). Observations were taken over 123 orbits, covering a period of 68.2 days: 1 January - 9 April, 2001. The dataset consists of 98×1300 s exposures in the F606W filter (*V* band) and 148×1300 s exposures in the F814W filter (*I* band), all taken in the same field of M4, about 6 core radii ($\sim 5'$) from the cluster center. This combined dataset represents the deepest ever imaging of a globular cluster. The primary purpose of these observations was to search for the faintest white dwarf stars in the cluster, however the data make up a time-series dataset that can be used to investigate the presence of variable objects in this particular field of M4.

2.1. Preprocessing and Combined-Image Photometry

The images were preprocessed according to recipes given in Stetson (1987) and Stetson et al. (1998). Crowding was not an issue on these images, due to their distance from the cluster center, as well as the high resolution of the *HST* images. A master star list, frame-to-frame coordinate transformations, and photometry of the combined image of the field were completed as discussed in Richer et al. (2002), which resulted in color-magnitude diagrams that reach apparent magnitudes of $V \sim 30$ and $I \sim 28$. These extremely faint data allow for

the study of variability in this globular cluster down to magnitudes which have rarely been probed.

2.2. Single-Image Photometry

To create time-series data for each star found in the M4 field, it was necessary to perform photometry on each individual exposure. To accomplish this, the following steps were taken: (1) the known frame-to-frame transformations were used to create a combined median image of the field for each chip on WFPC2. This was performed using the MONTAGE2 software written by Peter Stetson, which transforms the coordinates of each individual image to match a reference coordinate system, and then produces a combined image. (2) Once the combined median image was created, aperture photometry was performed on all objects using DAOPHOT. Subsequently, point spread function (PSF) photometry was performed using the ALLSTAR program in order to identify stellar centroid positions. This was done by employing PSFs built specifically for each chip and filter on WFPC2 by Stetson (2001). (3) The output photometry and frame-to-frame transformations were then provided to ALLFRAME, again written by Stetson, in order to perform PSF photometry on each individual exposure (Stetson 1994; Turner 1997). This software automates the PSF photometry of each individual exposure by using the frame-to-frame coordinate transformations. It also derives stellar centroids for each original image, and facilitates cross-identification of any given star between frames by assigning identification numbers to each star, which are consistent through all individual frames. Once this single-image photometry was completed, the location of any given star and its accompanying photometry was specified for every single exposure taken in the M4 field.

Since *HST* is above the Earth’s atmosphere, it is not subject to seeing effects experienced by its ground-based counterparts. However, it is susceptible to slight focus changes due to the telescope moving in and out of the Earth’s shadow as it orbits, which causes temperature fluctuations (i.e. breathing). As a result, the full width half-maximum (FWHM) of the stellar PSFs on the frames can vary slightly between individual images. The result is that small offsets in the magnitudes calculated from performing PSF photometry will exist from frame to frame. These must be corrected for before performing any analysis on the data. To accomplish this, the magnitudes that are output by ALLFRAME for every image on a given chip were compared to those of a reference image, which was chosen to be the first image taken in the data set⁸. The magnitude offset between frames was calculated by taking the

⁸Use of the combined median image as a reference was also explored, but there was a negligible difference

weighted mean of the magnitude difference for each star common to both frames.

The usual way of rejecting data points consists of fitting the distribution of magnitudes of a given star to a Gaussian profile, and throwing out any data points at a magnitude greater than 3σ or so from the mean of the distribution, and perhaps reiterating this process a number of times. When looking for variability, objects searched may include those which vary greatly in magnitude, such as eclipsing binary stars with deep minima, or supernovae. By performing this so-called “ $k\sigma$ clipping” type of data point rejection, data points that may be rejected could actually be caused by real effects due to a significantly varying object. In order to avoid the loss of potentially useful data, a “bad data point” is considered to be one which has a magnitude error which is significantly larger than the rest of the data points for the corresponding star. To illustrate how “significantly large” was defined, Figure 1 shows plots of root-mean-square magnitude (RMS or σ) vs. mean magnitude in I and V for each chip. It can be seen that for all of these chips and filters, the scatter of data points begins to increase significantly at a well defined “elbow” in the distribution, after which point the RMS grows rapidly with fainter magnitudes. With a few exceptions, the maximum scatter of the light curve of any star found in the data set is approximately 0.1 magnitudes. To be conservative, this is the value chosen as the cutoff magnitude error, so that any individual data point with an error above this value was rejected as a bad data point. Thus, no single data point that has an error larger than the RMS scatter of any light curve of almost any star in the dataset was used in the analysis.

The remaining data were used to create time-series magnitude profiles (light curves) of each star found. An example of a light curve from this dataset for a non-variable star is given in Figure 2. Note that there is a 44.4-day gap in the data. Analysis was then performed to determine if any of these stars demonstrated variability.

3. Expectations

As mentioned earlier, eclipsing binary stars are known to exist in globular clusters. For M4 in particular, seven W UMa binary stars thought to be cluster members were found by Kaluzny et al. (1997) in an 8.8×8.8 field centered on the cluster with apparent magnitudes reaching as faint as $V = 17.7$. The field observed in the current dataset is well within this area. However, unlike the above study, the magnitude range that can be probed for variability in the current study ranges from $20 \lesssim V \lesssim 26$, so all variables found in that

found in the final magnitudes and magnitude errors obtained, compared with those found through use of a single exposure as the reference image.

study are saturated on the current dataset. However, there is no reason to expect that the existence of binaries is exclusive to bright magnitudes. In a recent study of the core of the globular cluster 47 Tucanae (47 Tuc), which probed magnitudes as faint as $V = 25$, 11 detached eclipsing binaries and 15 W UMa systems were discovered in a sample of 46422 main sequence stars, resulting in an observed binary frequency of 0.056% (Albrow et al. 2001). In this study of M4, 2102 stars have been analysed. If no assumptions are made about the dependence of the distribution of binary systems with cluster radius, one would expect that only one or two binary stars should be discovered in the field observed based on the observed frequency in 47 Tuc. This already small number is decreased if it is assumed that the majority of binaries are expected to reside close to the cluster center due to mass segregation, since the M4 field was taken at about 6 core radii from the cluster center. The picture becomes even less optimistic considering that only 9 of the 15 W UMa eclipsing binaries found in the 47 Tuc study are below the main sequence turn-off point. However, 71 BY Draconis variables, which are thought to be members of binary systems, were also discovered, making up 0.15% of the sample. This converts to a slightly more optimistic expectation of 3 or 4 of these objects being discovered in the M4 field.

As a way of gauging the number of supernova events that are expected to be seen in the current dataset, a comparison is made to a recent study of the Hubble Deep Field (HDF), in which two supernovae were discovered (Gilliland et al. 1999). As with M4, the HDF was observed with the WFPC2 camera on *HST*, and just as deep, with a limiting magnitude of $I \sim 28$ (Flynn et al. 1996; Richer et al. 2002). However, unlike the HDF, M4 is close to the Galactic plane and ecliptic, and the images thus contain zodiacal light, in addition to many stars. This results in much higher background levels compared to the HDF. This significantly decreases the number of observable faint galaxies in the field. As will be discussed in section 7.2, 170 galaxies were identified in the M4 images. By contrast, ~ 2100 galaxies were identified in the HDF (Williams et al. 1996). Scaling the discovery of 2 supernovae in the HDF to the current dataset, it is estimated that ~ 0.08 extragalactic SNe would be expected in this set of images. It is of course not expected that any SNe will be found within the cluster itself – stars residing in M4 are very old relative to the lifetime of a star that eventually explodes in a type II supernova. The discovery of a type Ia supernova is a possibility, but a very unlikely one; the rate of type Ia SNe occurring in the Milky Way is thought to be of order one per 267 years (Binney and Merrifield 1998).

There also exists the possibility of discovering variable objects which have not yet been discussed, such as cataclysmic variables, flare stars, transiting planetary-sized objects, or perhaps a new species of variable star. Cataclysmic variables (CVs) are a special class of binary system with a white dwarf star as the primary and a low-mass main sequence star as the secondary. Here, the white dwarf is accreting matter from the secondary, which

has filled its Roche lobe, resulting in occasional outbursts of energy. Included as types of CVs are classical and dwarf novae. These objects are very unpredictable, making it difficult to quantify how many are expected to be seen in the M4 field. However, in globular clusters, which have a high frequency of stellar interactions, it is expected that an abundant population of CVs would be found (Di Stefano and Rappaport 1994; Gridlay et al. 2001; Knigge et al. 2002; Townsley and Bildsten 2002). A relatively small sample of stars may limit this population in the current observations, but the possible existence of CVs in this dataset is not discounted.

Flare stars are M or K-type stars with very strong magnetic fields, which undergo occasional and sudden outbursts of energy, causing their brightnesses to increase temporarily. Flare stars include the *BY Draconis* (BY Dra) variables. These stars are binary systems which are chromospherically active, and show enhanced magnetic activity, which is generally manifested visually as flaring or low-amplitude periodic variability due to starspots. As touched upon earlier, in the binary frequency study of 47 Tuc, 71 BY Dra variables were discovered with periods ranging from 0.4-10 days in the magnitude range $14 \lesssim V \lesssim 24.5$, comprising 0.15% of their sample of stars (Albrow et al. 2001). This converts into an expectation of finding about 3 or 4 BY Dra stars in the M4 field, assuming the distribution of these stars is more or less constant with cluster radius.

The main science driver for the above-mentioned study of 47 Tuc was to define the frequency of close-in gas giant planets orbiting main sequence stars (Gilliland et al. 2000). This study reported a null result, even though simulations that were carried out clearly show excellent sensitivity to planetary transits. However, the observations were centered on the core of 47 Tuc, which may be too hostile an environment for planets or protoplanetary disks to survive. The M4 images were taken far from the core of the cluster, where the number density of stars is much smaller, and may be a more suitable environment for planets to form. On the other hand, most extrasolar planets are found to be orbiting stars with relatively high metallicity. M4 is a more metal poor globular cluster than 47 Tuc, perhaps indicating that a smaller fraction of planets will be found in the current dataset. If the null result from 47 Tuc is any indication, it is expected that in the present study of M4, which contains only $\sim 4.5\%$ of the number of stars in the 47 Tuc dataset, no planetary transits will be found. In addition, planetary transits found by Charbonneau et al. (2000), and very recently by Konacki et al. (2003), show eclipse depths of $\sim 1\%$ for close-in Jupiter-size planets. For the star shown in Figure 2, which is typical of a relatively bright, non-variable star in this dataset, the scatter in its light curve is ~ 0.014 magnitudes. This is most likely too large to confirm a 1% eclipse depth should one exist in the light curve. On a more positive note, however, M4 is known to contain a millisecond pulsar with a planetary companion (Lyne et al. 1988; Backer 1993; Rasio 1994; Sigurdsson 1995; Thorsett et al. 1999). The presence of a

planet in this unusual system may be suggesting that planets are rather common in at least this globular cluster.

The stars for which planetary transits have been observed are stars of solar-like mass and radius. However, the magnitude range of the stars that we have examined for variability is $19 \lesssim V \lesssim 26$. This corresponds to a range in stellar masses of $0.6M_{\odot} \gtrsim M_{\star} \gtrsim 0.1M_{\odot}$. These stars have smaller radii than the Sun, and one would expect that for planetary occultations of such stars, the eclipse depth that would be seen in the star’s light curve would be significantly deeper than for the two transiting planets found to date. In fact, once the stellar mass goes down to $0.1M_{\odot}$, close to 100% eclipse depths could be expected.

4. Candidate Selection

After reducing the data and rejecting bad data points as described in section 2.2, variability searches were conducted on the light curves of the stars in the data set. Described in the subsections that follow are various criteria that were employed in order to narrow down the number of candidate variable stars in this dataset. After satisfying the criteria, any star that contained in its light curve less than six data points was immediately rejected. This may seem like a rather generous cutoff value, but when searching for possible supernova events, six points could be enough to determine if it is indeed a viable candidate. Stars were also excluded from the search list if:

- The image of the star is saturated on the CCD;
- The star is close enough to the edge of the image so that it can partly appear and disappear over time due to the observational dithering pattern;
- The stellar image is affected by light from a nearby saturated star; or
- The star is partially or exactly aligned with a diffraction spike of a bright or saturated star.

All remaining candidates that were not excluded due to the above criteria are presented and included in tables accompanying each subsection.

4.1. Statistical Outliers

One way to select potential variable stars is to use the magnitude dispersion of a given star’s light curve relative to the mean magnitude of that star. First, a simple identification

was made of outliers in standard deviation (RMS magnitude) as a function of magnitude. These stars have a larger scatter than is expected for stars of similar magnitude, and are thus potential variable star candidates. These RMS magnitude outlier stars, not including those rejected due to a lack of data as described in section 4, are shown in Figure 3, and candidates chosen by using this method are listed in Table 1. In this and other tables, coordinates of the objects listed are based on work on M4 by Ibata et al. (1999), and coordinates for stars not included in that study were calculated using the CCMAP and CCTRAN tasks on the IRAF analysis package.

While the above method of choosing variability candidates based simply on the scatter of the light curves of the stars in the sample is a good first pass in the candidate search, is not terribly robust against data corrupted by cosmic rays and warm pixels, which are quite common in *HST* images. A more robust candidate selection criterion that attempts to account for these effects is the variability index statistic formulated by Stetson (1996). Another attractive feature of this method is that it makes use of data in *all* filters employed in the dataset in determining the variability index statistic. What follows is summary of the method; further details can be found in the original paper.

The variability index J is given by:

$$J = \frac{\sum_{k=1}^n w_k \operatorname{sgn}(P_k) \sqrt{|P_k|}}{\sum_{k=1}^n w_k}. \quad (1)$$

Here, the user has defined n pairs of observations, each with an associated weight w_k . A pair is usually defined as two observations taken within some maximum separation in time, which is chosen by the user. It is important to note here that equation 1 also allows single observations to be used in the instances where a data point is not within the chosen date threshold of any other data point. P_k is the product of the normalized residuals of the two observations (denoted by the subscripts i and j) that form the k th pair, and is given by:

$$P_k = \begin{cases} \delta_{i(k)} \delta_{j(k)} & \text{if } i(k) \neq j(k) \text{ (observation pair);} \\ \delta_{i(k)}^2 - 1 & \text{if } i(k) = j(k) \text{ (single observation),} \end{cases} \quad (2)$$

where $\delta_{i(k)}$ (or $\delta_{j(k)}$) is the magnitude residual of a given observation from the weighted average of all observations *in the same bandpass*, scaled by the standard error:

$$\delta_{i(k)} = \sqrt{\frac{n}{n-1}} \frac{m_i - \bar{m}}{\sigma_m}, \quad (3)$$

where n is the total number of observations contributing to the mean, i.e., the number of observations taken in the same filter as the i th data point.

Rather than using σ -clipping techniques in an effort to reject bad data points from the light curve of a star, which can potentially remove a measurement that reflects a real variation in the brightness of an object, the stars are reweighted according to the size of their residuals as calculated in equation 3. To do this, the average magnitude \bar{m} in equation 3 is redefined as follows:

$$\bar{m}_{new} = \bar{m}_{init} \times \left[1 + \left(\frac{|\delta|}{a} \right)^b \right]^{-1}, \quad (4)$$

where \bar{m}_{new} is the new reweighted mean, and \bar{m}_{init} is the initial arithmetic weighted mean, which is multiplied by a weighting factor. This procedure is iterated until the mean and the individual weights stabilize. According to Stetson, experimentation with artificial corrupt datasets show that the effectiveness of this method is not very sensitive to the values of a and b above. Following values used by Stetson for *HST* data, we have adopted $a = b = 2$. For our purposes, we have considered two consecutive points as a pair if they are separated by no more than 0.03 days, which is typical of the spacing in time between data points within a given orbit of observations in this dataset. If this is not the case for any one data point, it is treated as a single observation in equation 2. Pairs of observations were assigned a weight $w_k = 1$ and single observations were assigned a weight of $w_k = 0.25$ in equation 1, following work by Mochejska et al. (2002), in which 47 low-amplitude variable stars were discovered in the open cluster NGC 6791.

Values of J were computed for every star, and those with values of J that were obvious outliers in the variability index distribution as a function of magnitude were considered variable star candidates. These distributions are shown in Figure 4, where stars selected as candidates are plotted as open circles. None of these stars passed the additional criteria described in section 4, and so no variable star candidates arose as a result of using this method.

4.2. Main Sequence and White Dwarf Sequence Outliers

As explained in Section 1, not many binary star sequences are found parallel to the main sequence in globular cluster CMDs. Looking at the color-magnitude diagram of M4 (Figure 5, left; (Richer et al. 2002)), one can see no obvious second sequence in the magnitude range observed, other than the expected faint white dwarf (WD) sequence. Nevertheless, there are stars that appear to be outliers to the main sequence, lying above it, or between it and the white dwarf sequence. The CMD on the right hand side of Figure 5 is the same as that on the left, but stars which obviously do not lie on the MS or WD sequence are plotted as open circles. Out of these stars, period searches were performed on those which were not

excluded according to the criteria listed in section 4. These remaining candidates are listed in Table 2.

4.3. ZZ Ceti Variables

The current dataset also includes white dwarf stars that are coincident with the ZZ Ceti instability strip. Figure 6 shows the M4 CMD, with the ZZ Ceti instability strip bordered by a black box. However, there is very little chance that any of the presently observed M4 stars would be identified as being variable. Firstly, the Nyquist frequency for this dataset corresponds to a period that is larger than the typical period for ZZ Ceti pulsators (~ 1000 s). The Nyquist frequency ν_n is the highest frequency of variability detectable, given the time sampling of the data. For evenly spaced data, it is given by $\nu_n = 1/2\Delta t$, where Δt is the spacing in time of the data. For a case such as the current dataset, where the data is unevenly spaced, a pseudo-Nyquist frequency can be calculated with Δt being the minimum spacing between any two data points. For this dataset, this minimum spacing is 843 seconds, yielding a Nyquist frequency of 5.93×10^{-4} s $^{-1}$, which corresponds to a period of 1687.5 seconds, or 0.02 days, which is significantly larger than the typical ZZ Ceti period.

Independent of the Nyquist frequency is the consideration of the exposure times of the individual images, which are 1300 seconds for each single observation. This is on the order of the typical ZZ Ceti period. Any variability in these stars would be “washed out”, since the integration time of each observation is too long to capture the star at various stages of its pulsation cycle.

However, it is useful to list the stars which are thought to lie on the ZZ Ceti instability strip. Future observations can be made specifically to study these objects. Table 3 lists these ZZ Ceti variable star candidates as well as their coordinates, magnitudes and colors, and Figure 7 presents finder charts for these three candidate variables.

5. Periodicity Analysis

Ever since the landmark paper by Stellingwerf (1978) describing the technique, phase dispersion minimization (PDM) has been used extensively and successfully in the discovery of countless numbers of variable stars and binary systems. It is one of the favourite methods used by astronomers in determining variable star periods. As with most techniques, it has its advantages and disadvantages. Unlike Fourier transform analysis, which is particularly well-suited for sinusoidal-type pulsations, it is not sensitive to the shape of a star’s light

curve. In addition, its implementation is very straightforward. However, determination of the statistical significance of results obtained from use of PDM is not so simple, as is the case for Fourier techniques. It has been shown that the PDM probability distribution does not follow an F distribution (Schwarzenberg-Czerny 1997), as originally thought. Methods used here to estimate the reliability of findings made by PDM analysis will be discussed in the next section.

As an example of this analysis, the light curve of a simulated data set with known period and amplitude is shown in Figure 8. This is a sine curve with identical time sampling to the M4 I -band data (148 data points), with a period of 0.42 days (within the range expected for close binary systems) and amplitude of 0.2 magnitudes. The magnitude errors on each data point are typical of the noise levels found in the dataset. The top half of Figure 9 shows the Θ^9 distribution obtained by performing PDM analysis on the data. The lower half of the figure shows the phase-folded light curve for the period found to be associated with the lowest calculated value of Θ . There is no question that the analysis was successful in finding the correct period for this light curve (the other minima in the periodogram correspond to aliases of the input period). PDM analysis was performed on all stars in the dataset, and particular attention was paid to candidate variable stars.

6. Reliability Tests

In an effort to understand the reliability of the PDM analysis performed on candidate variable stars, a number of artificial stars were created by sampling different types of variable star light curves at the same observation times as the M4 dataset. These artificial stars were then added to the WF2 images, and PDM analysis was performed on the light curves extracted from the resulting images.

Sinusoidal light curves were simulated with a range of periods, amplitudes, and magnitudes. The range of magnitudes simulated were $17 \leq I \leq 28$ and $19 \leq V \leq 28$. The bright end of these ranges correspond to the saturation limits of the dataset in each badpass. The faint end corresponds to the faintest magnitude reached in the combined I image. Six periods were simulated: 0.085, 0.16, 0.42, 2.1, 5.6, and 15.6 days. The shortest period simulated corresponds to a value just above the Nyquist frequency for this dataset (see section

⁹ Θ is the ratio of the total phase-folded light curve variance, calculated from the individual variances of a given number of phase bins, to the variance of the entire light curve. For the correct trial period of a variable star, Θ will be much less than neighboring trial periods, hopefully near zero. Incorrect trial periods will have values close to one.

4.3), and the longest period simulated corresponds to approximately the period over which the data was taken before the occurrence of the 44.4-day gap in the observations. Finally, sinusoids with amplitudes of 0.002, 0.02, and 0.2 magnitudes were simulated. In all, 20181 sinusoidal light curves were simulated for each filter. An example of the artificial sinusoids are shown in Figure 10 for the case of an amplitude of 0.2 magnitudes in I , with a period of 0.42 days.

In addition, two types of eclipsing binary star light curves were simulated. The binary star curves were simulated by employing the widely-used Wilson-Devinney (W-D) code for eclipsing binary star light curve analysis (Wilson and Devinney 1971). However, for the purposes of this study, the full capabilities of the W-D code were not needed, and it simply served as a light curve generator. Using the code, Algol and a W UMa-type systems were simulated, each with a 0.42-day period. The simulated Algol system has an orbital inclination (i) of 67° , a relative orbital ellipse semimajor axis length (a) of $351.6 R_\odot$, and a primary eclipse depth of ≈ 0.3 magnitudes. The simulated W UMa system has $i = 47.5^\circ$, $a = 1.88 R_\odot$, and a primary eclipse depth of ≈ 0.2 magnitudes. A period of 0.42 days was chosen because it exhibits a case of full phase coverage for this dataset, representing a good scenario for diagnostics performed for the purpose of understanding the reliability of the PDM analysis of this dataset. In addition, it is within the range of periods typical of close binary stars. In all, 961 stars were simulated and added into the images for each of the Algol and W UMa-type light curves in each filter. Examples of these artificial star light curves, phased folded to their corresponding input periods, are shown in Figures 11 and 12.

The light curve data was used in conjunction with the ADDSTAR program in DAOPHOT (Stetson 2001) to add artificial stars to the actual M4 images at different magnitudes. This ensured that the output light curves would have noise levels typical of real stars in the image with similar magnitudes. Photometry was performed on these artificial stars in the same way as on the original images, as described in section 2.2.

A recovered period within 1% of the correct input period was considered to be a successful recovery. Results from the simulation of the artificial sinusoidal light curves are shown in Figure 13. For the curves in both bandpasses with an amplitude of 0.2 magnitudes, PDM analysis recovers the input period almost 90% of the time down to a magnitude of 24 in I and 26 in V (at which point the recovery rate drops to $\sim 64\%$ at its lowest). Over the range of periods simulated, there is no dependence on period here apart from the 0.085 and 15.4-day cases. This gives an idea of the periods to which the PDM analysis is sensitive at this amplitude given the time sampling of this dataset. For the case of light curves with 0.02 and 0.002-magnitude amplitudes, the ability of PDM analysis to recover the correct input period is significantly lessened. For an amplitude of 0.02 magnitudes or less, the recovery

rate in I -band is very poor regardless of period or magnitude. For V -band, the period search is also discouraging, although the 0.42 and 2.1-day period recovery rate is slightly higher for brighter stars. This is most likely due to the higher signal-to-noise obtained in the V filter. In the case of the 0.002-magnitude amplitude curves, the PDM analysis recovery rate is even less successful, where, regardless of period or magnitude of the light curve, the input periods are generally not recovered. This is not surprising, since the scatter of the light curves is on the order of this amplitude or greater (see Figure 1), even for bright stars.

The results of the tests for the artificial binary star light curves are found on Tables 4 and 5. These tables show the number of stars added at each magnitude, the number recovered, and the percentage of those stars recovered with Θ values corresponding to four different groups of periods. The first group is simply the correct input period (0.42 days), the second group is half the input period, and the third group is $\frac{3}{2}$ the input period. It was found that these are the three major groups within which the periods of the artificial binary stars were recovered. The fourth group corresponds to periods that do not fall into any of the three previous categories. The reasons for the PDM analysis finding periods at half or $\frac{3}{2}$ the input period is evident once one observes the results of the analysis for a couple of cases. As an example, Figure 14 shows the results of PDM analysis performed on a W UMa-type light curve added to the V -band images. This artificial star was found by PDM analysis to have a period of ~ 0.21 days (half the input period). It is expected that a strong signal would be found at this period, especially in the case of the W UMa light curves simulated here, which typically have eclipse minima that, while unequal in depth, are similar in width. However, inspection of the periodogram shows that there is a significant drop in Θ at the correct period of 0.42 days, and is comparable to the value of Θ corresponding to a 0.21 day period. The bottom two plots show the phase-folded light curves for each of these periods. One can see that while the curve corresponding to a 0.42 day period seems to have less scatter, the curve corresponding to the 0.21 day period seems to show less variation over the unit interval. The reason the PDM analysis chooses a lower value of Θ for the 0.21 day period instead of the 0.42 day period is due to the bin structure used in the analysis. For a bin length of 0.2 in phase (the bin length used), the variance of each bin will be larger on average for the 0.42-day folded light curve. Using a small bin length would no doubt lower the variance of each phase bin for the 0.42 day curve, but due to the amount of data available from these observations, there would be very few data points within each phase bin upon which to base a result. Thus, although the lowest value of Θ did not correspond to the input period, the bin structure that was used does work, since a quick inspection of the periodogram obtained for the light curve demonstrates that the input period was indeed recovered; it does correspond to a significantly low value of Θ compared to neighbouring trial periods. This was generally not an issue for the I -band images, since the data taken in

this filter has greater time sampling than in V . Thus, a period recovered that was equal to, one half of, or three-halves of the input period was considered a successful recovery for the artificial binary star light curves.

7. Searches for Non-Periodic Variable Stars

In addition to periodic variables, there may exist objects in the M4 field that vary in magnitude, but not periodically. There is also the possible presence of objects whose period is too long compared with the time frame in which the observations were taken (or too short relative to the time sampling or exposure time), so that their periodicity may not be evident. Clearly, tools such as PDM are not useful in searches for these objects. Non-periodic objects include, but are not limited to: transits of stars by planetary-sized or other objects, cataclysmic variables, supernovae, and flare stars. The variability candidates chosen by some of the methods outlined so far in this section (MS/WD outliers and variability index, to be specific) *are* valid for these cases and those candidates chosen by these methods were used to search for the existence of non-periodic variability in the M4 field.

7.1. Planetary Transits and Median-Smoothed Light Curves

As an estimate of the typical period lengths that can be expected to be seen with this dataset, we take an example of a Jupiter-sized planet. From the reliability tests described in section 6, we can expect to find periodic transits that have eclipse depths of about 20%. To get a 20% dip in the light curve of such a system, the radius of the parent star must be $\lesssim 0.2R_{\odot}$. This translates into a mass $\lesssim 0.23M_{\odot}$ (Montálban et al. 2000), and a magnitude $V \gtrsim 23.2$ for this dataset. We set a minimum detectable transit time ~ 5600 s based on the minimum separation in time between three consecutive exposures in the light curve. We estimate the orbital speed implied by such a transit by calculating the length of the transit to be the time it takes for the planet to pass from 2nd contact to 3rd contact. This implies a maximum orbital speed of 31.6 km s^{-1} . Assuming a circular orbit ($v_{orb} = 2\pi a/P$), the orbital period is then given by:

$$P = \frac{2\pi G(M_{\star} + M_{pl})}{v_{orb}^3} \simeq 71 \text{ days.} \quad (5)$$

This is longer than the length in time over which the dataset was taken, so only one eclipse would be expected to be found. This is also a lower limit to the period, for the following reasons. From section 6, the lower magnitude limit at which we successfully recover periods

over 90% of the time is $V \sim 26$. This corresponds to $\sim 0.1M_{\odot}$ for main sequence stars. A lower mass star has a smaller radius, and so the orbital velocity the planet must be slower in order to have a transit time that can be detected in this dataset, which results in a longer orbital period. The same argument holds for a higher orbital inclination, since the separation between second and third contacts is smaller. Thus, periodic signatures of planetary transits would not likely be found for this dataset. However, searches for single transits were carried out.

One method used to search for one-time planetary transits and variable star candidates with non-periodic variability involved smoothing the light curve of each star found in the dataset. This was done by replacing each data point in the light curve with the median of that point and its four nearest neighbouring points. This has the effect of reducing the scatter in the light curve, so that real variations in the light curve would be pronounced.

This method was executed as follows. The faintest data point in each median-smoothed light curve was selected. The ratio of the difference in magnitude between that point and the mean magnitude of the light curve to the RMS scatter of the light curve was calculated. Outliers to the distribution of this ratio represent data points that deviate more than is expected from the scatter of the smoothed light curve, which would indicate the possibility of a real temporary variation in the star’s light curve. However, all the outliers found were simply due to saturated stellar images, diffraction spikes, or the star being too close to the edge of the image, causing it to disappear and reappear in the frame over time. Thus, no candidates for planetary transits, or other type of non-periodic variable star, were found using this method.

7.2. Searching for Supernovae

In addition to the median smoothing of light curves, additional techniques were employed in the search for possible supernovae (SNe) occurring in the M4 field. Within the dataset, there is a 44.4-day gap in the data. For this section, and further discussions pertaining to searching for supernova with this dataset, *epoch 1* will refer to the data taken before this gap, and *epoch 2* to the data taken after the gap. The data taken during epoch 1 and epoch 2 were combined separately for each bandpass using MONTAGE2, and PSF photometry was performed on each resulting image using DAOPHOT and ALLSTAR in exactly the same way as described in section 2.2. The combined epoch 1 images used 100 images in I and 66 in V , taken over 14 days. The combined image for epoch 2 used 48 images in I and 32 in V , taken over 9 days. Three methods employing these combined images were used to search for supernova candidates, and are described as follows.

The first method involved searching for stars which were found on the combined image of one epoch, but not on the other. All of the stars that were chosen as candidates as a result of this search turned out to be either saturated, near to the edge of the image, or too faint to be found on the epoch 2 image with enough signal-to-noise to be considered a real detection. By contrast, the second method used stars that were common to both frames. The difference in magnitude between epoch 1 and epoch 2 was calculated for each star, forming a tight distribution about a zero magnitude difference, with scatter increasing towards fainter magnitudes, as expected. Outlier stars in this distribution were chosen, since they deviate significantly from the expected magnitude difference compared with other stars of similar magnitude. The distribution for each chip and filter, as well as candidates selected, are shown in Figure 15. None of the candidates resulting from this search passed the exclusion criteria described in section 4.

The third and final method employed in searching for supernovae in the M4 data involved examining the background galaxies found in the images and comparing them from one epoch to the next. Galaxies were identified through the use of two methods. The first method involved using the SExtractor program (Bertin and Arnouts 1996), which uses neural network software to identify galaxies separately from stars in an image. The second method was simply to look for “fuzzy” objects that SExtractor was not able to classify on the images. The comparison between epochs was performed by subtracting the combined epoch 2 image from the combined epoch 1 image, in the hopes of discovering residual flux in the subtracted image, possibly indicating the presence of a supernova. Before subtracting the two images, the signal due to the sky background was removed from each image, and the total flux for each combined image was normalized. This is necessary since the amount of images that make up the combined epoch 1 image, and hence its total flux, is greater than for the epoch 2 image. The MONTAGE2 software described in section 2.2 performs this sky subtraction and flux normalization for each combined image it creates.

The subtracted images produced were not very good, and it is thought that this is due to the poor sampling of the point spread function of stars in *HST* images. In an attempt to improve the quality of the subtracted images, the combined images were created again as described above, but this time after resampling the pixel grids of the single images to increase the resolution of the point spread function. This was accomplished again using MONTAGE2, which allows the user to expand the images in this way. This process is similar in concept to the “drizzling” technique (Fruchter and Hook 2002). The PC chip was expanded by a factor of two, and the WF2, WF3, and WF4 chips were each expanded by a factor of three. The quality of the resulting subtracted images was improved, but not by a significant amount. However, it seemed that the subtraction did work well for faint objects, which included most of the galaxies found in the field. Several of the galaxies contained bright cores that did not

subtract very well, but they were in the minority.

The results of subtracting the epoch 2 image from the epoch 1 image are shown for *I*-band data of each chip in Figures 16 - 19. Shown in these figures are three columns of images, which are subsets of the original epoch 1, epoch 2, and (epoch 2 – epoch 1) images, and are centered on the coordinates of each galaxy identified, with each row corresponding to a different galaxy. Each image is a 20×20 pixel subset for the PC chip, and a 30×30 pixel subset for the WF2, WF3, and WF4 chips. There is no evidence for any residual flux greater than about 1σ above (or below) the noise levels for the image, except in cases where the nucleus of the galaxy was too bright, and the quality of the subtraction was poor. However, this negative result may still be interesting. Some of these bright nuclei show stellar-like light profiles, perhaps indicating the presence of active galactic nuclei. This would make these galaxies interesting objects for possible further study.

8. Results and Discussion

After candidates were selected as described in section 4, their light curves were examined more closely and were analyzed using PDM to search for periodicity. Of all the variable star candidates listed in the tables in the previous sections, only one of these stars (PC, ID #97) showed real signs of variability in its light curve. Even for this remaining candidate star, indicators of periodicity were not significant enough to be conclusive. It is therefore possible that this remaining candidate is non-periodic, or else there is not enough data in the light curve of that star to decisively find a period for it through PDM analysis.

In what follows, results of the PDM reliability tests, and of the variable star searches will be presented and discussed. The results obtained from analysis of the remaining candidate star will be presented in section 9.

8.1. Reliability Tests

Tests of the reliability of the PDM analysis performed on this dataset, and the outcome of these tests, are outlined in section 6. These results suggest that for artificial binary stars added to the images, the PDM analysis is highly successful in recovering their input periods, down to limiting magnitudes of $I \sim 24$ and $V \sim 25$, at which point only half of stars are recovered with the correct input period. For the W UMa-type light curves, these limits are $I \sim 24$ ($\sim 75\%$ recovered) and $V \sim 25$ ($\sim 97\%$ recovered). Below these limiting magnitudes, almost none of the stars were recovered with light curves consisting of more than 6 data

points (see section 2.2), let alone with the correct input period. No variable stars resembling a binary star light curve were actually found, so it is thought that there are no eclipsing binary systems observed with periods on the order of half a day (which have good phase coverage given the time sampling of this dataset) for $19 \lesssim V \lesssim 25$ and $17 \lesssim I \lesssim 24$, since the simulations show that these types of stars can be found decisively. Binaries with periods of this length are typical of contact binary stars, which include the W UMa systems. In addition, the successful recovery of sinusoidal light curves down to $I \sim 24$ and $V \sim 26$ seems to indicate that variable stars with sinusoidal-type pulsations of similar amplitude (~ 0.2 magnitudes) and covering a wide range of periods are nonexistent for $19 \lesssim V \lesssim 26$ and $17 \lesssim I \lesssim 24$. The limiting regions in the CMD of M4 for successful binary and sinusoidal light curve recovery are shown in Figure 20. Of course, there is the possible presence of variable stars in the M4 field with periods having poor phase coverage in our dataset. In these cases, PDM analysis would not be a very effective discovery tool.

8.2. A Lack of Variability

The previous sections discuss efforts made to search for variable objects in a field 6 core radii from the center of the globular cluster M4, observed with the *Hubble Space Telescope*. Results from these searches indicate that there are most probably no eclipsing binary stars in the field observed with periods ~ 0.5 days and amplitudes on the order of 0.2 magnitudes, down to limiting magnitudes of $V \sim 25$ and $I \sim 24$, based on simulations of Algol and W UMa-type light curves. This is consistent with a lack of contact binary systems, which have periods on the order of half a day. Searches for other types of periodic variable star have also yielded no candidates.

It can also be concluded that there are most likely no periodic variables with sinusoidal-type variations in the field with periods from about 0.1 to 6 days and 0.2-magnitude amplitudes, down to limiting magnitudes of $V \sim 26$ and $I \sim 24$, based on analysis of simulated sinusoidal light curves. In addition, a search for variable stars with non-periodic light curves found only one possible candidate.

The lack of eclipsing binary stars in the field can be explained in a number of ways. Firstly, it may be that any binaries that are present in this field are face-on relative to the line of sight, although this possibility is an unlikely one. Another reason may be the fact that the observations were taken in a field that is considerably distant from the core of M4. It is expected that mass segregation in the cluster will, over time, preferentially cause binary systems to sink toward the cluster center, since binary stars are typically more massive on average than single stars. This may not have left many binary systems at the large cluster

radius that was observed in this study. However, a considerable number of $\sim 0.6 M_{\odot}$ white dwarf stars are seen in the field (Hansen et al. 2002), as are main sequence stars up to $\sim 0.65 M_{\odot}$ (Richer et al. 2002), so it is not unreasonable to expect, for example, binary star systems comprised of $2 \times 0.3 M_{\odot}$ stars in that same field. Another possibility is that due to the high-density environment of globular clusters, low-mass binaries are more prone to disruption before they have the opportunity to harden over time through interaction with third bodies. Conversely, the relatively large numbers of blue straggler stars in globular clusters (30 have been found in M4 (Rucinski 2000)), may represent the coalescence of many low-mass binary systems which have acted as a heat source to the cluster in preventing core collapse. This could reduce the number of binaries expected in this magnitude range. However, the real explanation for the lack of eclipsing binaries in this sample may simply be small-number statistics. As speculated in section 3, based on the low fraction of stars in the study of 47 Tuc found to be in binary systems, the predicted number of objects recoverable in these data was low to begin with.

The small number of background galaxies observable in the M4 images is the most probable reason that no supernovae were found in the field observed. Previous studies of the Hubble Deep Field, whose images are comparable in depth to the M4 field, yielded a discovery of two supernovae (Gilliland et al. 1999). Due to the substantially larger background flux in the M4 observations compared to that of the HDF (see section 3), considerably fewer galaxies were observable, making it unlikely that any supernova would be found in these observations.

9. Remaining Candidate

In the above summary of results, an otherwise firm declaration of a null result for the presence of variability in this field has been modified by phrasing such as *most probably* and *most likely*. This is due to the still unresolved issue of the remaining candidate star found in the PC field of the observations. There is no clear reason that this star should not be considered as variable: it is relatively bright, it is not close to any image defects (such as cosmic rays or diffraction spikes from saturated stars) and is far from the edge of the image. Figure 21 shows a combined *I*-band image of the PC chip observations, on which the star in question is circled. In addition, it has been identified as a cluster member by its proper motion. An apparent peak in magnitude is seen in its light curve (Figure 23) in *both bandpasses at the same time*, further supporting the claim that this object is indeed variable. A clear second peak in brightness is not seen. This could mean that the star is not periodic, however, it may very well be that this object has a period such that a second peak

occured during a gap in the observations. Inspection of its light curve seems to indicate a possible period in the range of 5 - 9 days, but periodicity analysis performed on this star was inconclusive (see section 9.1).

This star has a magnitude $V = 22.6$ mag and color $V - I = 0.71$ mag, which places it at the bright end and just red of the white dwarf sequence in the CMD of M4, as shown in Figure 22. There is another star next to this candidate on the CMD. This star (ID #1), also found on the PC chip image, was very close to the edge of the frame. Its partial appearance and disappearance from the field over time, due to the dither pattern, was responsible for the observed variations in its light curve, causing it to be flagged as a possible variable star candidate.

The light curve of the potential variable star is shown in Figure 23, and is displayed in two sets of rows, which show the light curve data for each filter in which the observations were taken. The first set shows the data before the 45 day gap in the observations, and the second set of rows shows the data after this gap. The reason for presenting the data in this way is to highlight what is perhaps its most obvious feature in being a candidate variable star: the light curve seems to show the same behaviour in *both* bandpasses. This is seen much more clearly in the median-smoothed light curve of this star, shown in Figure 24. This was not seen in the light curve of any other candidate star. The notable feature in the light curve is the apparent rise in amplitude by ~ 0.1 magnitudes, seen within the first few days of the onset of data collection. If the light curve is periodic, it would seem to have a period of approximately 7 or 8 days, but would probably have to be modulated in amplitude over time in order to explain the lack of additional amplitude peaks.

9.1. Phase Dispersion Minimization Analysis

The results obtained from period searches on the candidate star using PDM analysis were not encouraging. None of the periodograms derived from this process showed any of the candidate stars to have a period with a corresponding value of Θ that was significantly lower than one, compared to other trial periods. Shown in Figure 25 are the results of the PDM analysis performed on the remaining candidate variable star. Trial periods of 4-10 days were searched, which is the range of possible periods that one might expect by examining the light curves in Figure 23. On the top half of Figure 25 the Θ periodograms obtained for this trial period range are shown, and indicated are the periods that are associated with the lowest value of Θ for data taken in each filter. The bottom half of the figure shows the light curve of the star in each bandpass, phase-folded into the period corresponding to the minimum value of Θ found. As with the rest of the stars probed, the Θ distribution does not seem to venture

far below a value of one. This could be because, as argued at the beginning of the section, the candidate is perhaps a non-periodic variable star, or has a period that is long compared to the duration of the observations. Another reason may be that a second (or third) rise in amplitude may have occurred during the 44.4-day gap in the observations. In any case, the observations of this star leave a great deal of room for speculation and interpretation, which will be presented in the following section. However, as with the light curves shown for this star in the previous section, the periodograms show a very similar structure for the light curves obtained from both the I and V -band data. This is encouraging, even though no definite period was found, because it seems to indicate that the light curves corresponding to observations in both filters follow similar trends in their progression over time, which is a feature not seen in the other candidate stars.

9.2. Discussion

The location of this star in the color-magnitude diagram, as shown in Figure 22, indicates that it may be a binary star, composed of a low-mass main sequence star and a white dwarf. In order to investigate this possibility further, a simple decomposition of this candidate into two stars was performed, by investigating the magnitudes and colors of two separate stars, lying on either the main sequence or white dwarf sequence, that would be needed to produce a single observed star of magnitude and color similar to this candidate ($V = 22.64$, $V - I = 0.706$). This gives further insight as to the types of stars that might exist in a binary system found in the position of the candidate star on the CMD of M4. The composite magnitudes of such a binary system were calculated as follows:

$$V_{comp} = -2.5 \log [10^{(-0.4V_1)} + 10^{(-0.4V_2)}] \quad (6)$$

$$I_{comp} = -2.5 \log [10^{(-0.4I_1)} + 10^{(-0.4I_2)}], \quad (7)$$

where the subscripts 1 and 2 refer to each star in the hypothetical system. We find that a binary system consisting of a white dwarf with magnitude and color $V \sim 22.7$, $V - I \sim 0.4$ and a faint, late-type main sequence companion star, with upper limits to its magnitude and color of $V \gtrsim 26.8$ and $V - I \gtrsim 3.4$, respectively, result in an object with a position on the CMD that is very near to that of the candidate star. This is illustrated in Figure 26. The positions of the two speculated binary star constituents are shown as the smaller open circles, and the resulting binary is shown as a filled circle. A large open circle is centered on the position of the actual candidate star. As one can see, the composite star is very close to the position of the candidate. Because of the proximity of the candidate variable to the white dwarf cooling sequence, it was expected that such an object would be dominated in luminosity by a white dwarf. The position of the hypothetical lower main sequence constituent would

indicate that this object could be a late M-type star. However, the magnitude and color found for this companion are lower limits, since any companion that is fainter on the main sequence contributes little to the hypothetical binary system. It is then possible that this companion could be an even fainter, lower-mass main sequence star.

It may be possible that this object is a cataclysmic variable (CV). It is thought that such objects can be identified in the color-magnitude diagrams of globular clusters, between the main sequence and the white dwarf sequence (Townsley and Bildsten 2002). In addition, those that are found close to the white dwarf sequence will be dominated in magnitude by the white dwarf component. This scenario is very similar to what has been found through the decomposition of the candidate object as described above. A search for CVs has been performed on this dataset by paying specific attention to those stars that fall between the MS and WD sequence. In addition, these stars were probed for possible eclipses by first normalizing and then combining the I and V light curves for each of these stars, and performing PDM analysis on these combined light curves. No CV candidates have resulted from this search.

The light curve of the object does not seem to show the characteristics of an eclipsing binary system. The possibility does exist that it is a face-on binary system that includes a BY Draconis variable. The period range of 0.4-10 days of the BY Dra stars found in the 47 Tuc study does not discount this as a possibility. In addition, that study reported amplitudes for these stars ranging from $V \sim 0.001 - 0.061$. This is not much smaller than the ~ 0.1 magnitude increase seen in the candidate object's light curve.

It is difficult to say with any certainty whether this object is a BY Dra variable. Further simulations were performed on 625 artificial sinusoidal light curves with an amplitude of 0.09 magnitude with $V = 22.0 - 25.0$ and $I = 20.0 - 23.0$; these are magnitude ranges within which the candidate star is observed. They were given an input period of 7.0 days, as this is within the range of periods for the star that its light curve would seem to indicate. These stars were added to the frame and analyzed as described in section 6. Results of the PDM analysis performed on these light curves show that *all* of the input light curves were recovered with the correct input period. This indicates that in all probability, this candidate is not periodic, or else it has a period that is too long to be detected with PDM analysis. In this case, more data would be needed to obtain full phase coverage in order to determine the nature of this object's variability.

Yet another possibility is that the observed increase in brightness is due to flaring on the star's surface, which would not necessarily be periodic, thus explaining the null result of the PDM analysis. However, this is unlikely, since the timescale typical of stellar flares rising to maximum brightness and diminishing is on the order of hours, whereas the rise in

amplitude in the light curve of the candidate star seems to last for days.

10. Closing Remarks

While this research did not produce any confirmed discoveries of variability in the magnitude range $V \sim 20 - 26$ for M4, it is far from having been fruitless. Firstly, there is one interesting candidate variable, for which it seems that more observations will be needed to identify its nature. However, with the nature of this candidate object unresolved, we can place an upper limit for the observed binary fraction for this study at 0.05%, within the magnitude ($19 \lesssim V \lesssim 26$ and $17 \lesssim I \lesssim 24$), amplitude ($\Delta V \gtrsim 0.1$ magnitude), and period ($0.16 \text{ days} \lesssim P \lesssim 7.0 \text{ days}$), values to which we were sensitive.

The identification of the white dwarf stars in the M4 field suspected of being ZZ Ceti variables may prove to be of considerable value. The discovery of such stars in a globular cluster is of the utmost importance to understanding the chemical structure and evolution of population II white dwarfs, which currently suffers from a lack of observational data.

We are grateful to Robert E. Wilson for providing the Wilson-Devinney code, and to Puragra Guhathakurta for several very useful discussions on various aspects of this work. J. S. K. received financial support during this work through an NSERC PGS-B graduate student research grant. H. B. R. and G. G. F. are supported in part by the Natural Sciences and Engineering Research Council of Canada. H. B. R. extends his appreciation to the Killam Foundation and the Canada Council for the award of a Canada Council Killam Fellowship. R. M. R. and M. M. S. acknowledge support from proposal GO-8679 and B. M. S. H. from a Hubble Fellowship HF-01120.01 both of which were provided by NASA through a grant from the Space Telescope Science Institute which is operated by AURA under NASA contract NAS5-26555. B. K. G. acknowledges the support of the Australian Research Council through its Large Research Grant Program A00105171.

REFERENCES

Albrow, M. D., et al. 2001, *ApJ*, 559, 1060

Backer, D. C. 1993, in *ASP Conf. Ser.* 36, *Planets around Pulsars*, ed. J. A. Phillips, S. E. Thorsett, & S. R. Kulkarni (San Francisco: ASP), 11

Bertin, E. and Arnouts, S. 1996, *A&AS*, 117, 393

Binney, J., and Merrifield, M. 1998, Galactic Astronomy, Princeton: Princeton University Press

Charbonneau, D., Brown, T. M., Latham, D. W., and Mayor, M. 2000, *ApJ*, 529, L45

Di Stefano, R. and Rappaport, S. 1994, *ApJ*, 423, 274

Flynn, C., Gould, A., and Bahcall, J. N. 1996, *ApJ*, 466, L55

Fruchter, A. S., and Hook, R. N. 2002, *PASP*, 114, 144

Gilliland, R. L., Nugent, P. E., and Phillips, M. M. 1999, *ApJ*, 521, 30

Gilliland, R. L., et al. 2000, *ApJ*, 545, L47

Grindlay, J. E., et al. 2001, *Science*, 292, 2290

Hansen, B. M. S., et al. 2002, *ApJ*, 574, L155

Hut, P., et al. 1992, *PASP*, 104, 981

Ibata, R. A., et al. 1999, *ApJS*, 120, 265

Kaluzny, J., Thompson, I. B., and Krzeminski, W. 1997, *AJ*, 113, 2219

Knigge, C., et al. 2002, *ApJ*, 579, 752

Konacki, M., Torres, G., Jha, S., and Sasselov, D. D. 2003, *Nature*, 421, 507

Lyne, A. G., Biggs, J. D., Brinklow, A., Ashworth, M., and McKenna, J. 1988, *Nature*, 332, 45

Mochejska, B. J., Stanek, K. Z., Sasselov, D. D., and Szentgyorgyi, A. H. 2002, *AJ*, 123, 3460

Montálban, J., D'Antona, F., and Mazzitelli, I. 2000, *A&A*, 360, 935

Rasio, F. A. 1994, *ApJ*, 427, L107

Richer, H. B., et al. 1997, *ApJ*, 484, 741

Richer, H. B., et al. 2002, *ApJ*, 574, L151

Rubenstein, E. A., and Bailyn, C. D. 1996, *AJ*, 111, 260

Rucinski, S. M. 2000, *AJ*, 120, 319

Schwarzenberg-Czerny, A. 1997, *ApJ*, 489, 941

Sigurdsson, S. 1992, *ApJ*, 399, L95

Stellingwerf, R. F. 1978, *ApJ*, 224, 953

Stetson, P. B. 1987, *PASP*, 99, 191

Stetson, P. B. 1994, *PASP*, 106, 250

Stetson, P. B. 1996, *PASP*, 108, 851

Stetson, P. B., et al. 1998, *ApJ*, 508, 491

Stetson, P. B. 2001, User's Manual for DAOPHOT II, Victoria: Dominion Astrophysical Observatory

Thorsett, S. E., Arzoumanian, Z., Camilo, F., and Lyne, A. G. 1999, *ApJ*, 523, 763

Townsley, D. M., and Bildsten, L. 2002, *ApJ*, 565, L35

Turner, A. M. 1997, Cooking with ALLFRAME: Photometry and the H_0 Key Project, Victoria: Dominion Astrophysical Observatory

Williams, R. E., et al. 1996, *AJ*, 112, 1335

Wilson, R. E., and Devinney, E. J. 1971, *ApJ*, 166, 605

Yan, L., and Mateo, M. 1994, *AJ*, 108, 1810

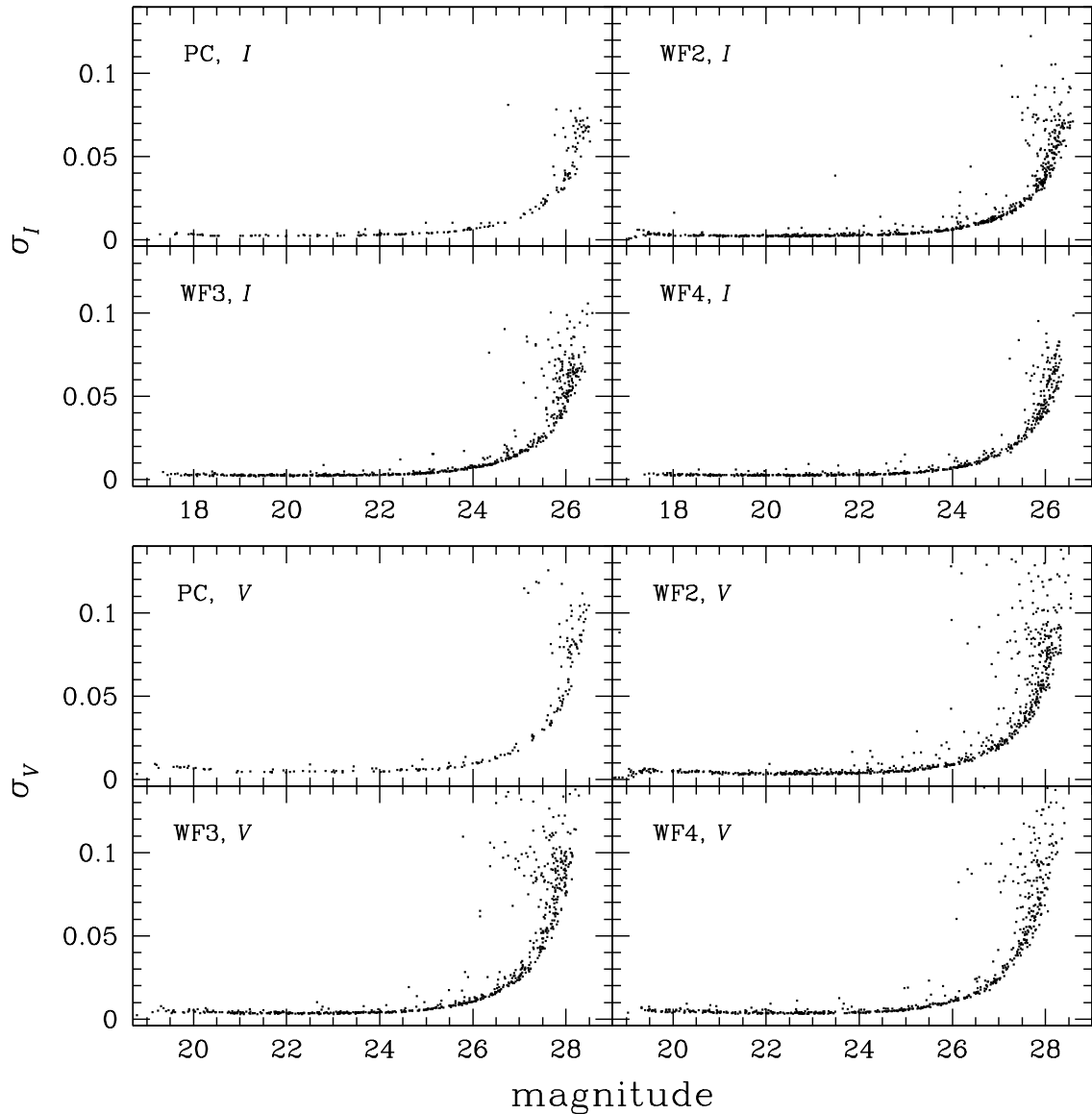


Fig. 1.— Graph of RMS magnitude as a function of magnitude for stars found in each chip of WFPC2 in the M4 images. Each distribution has a well-defined “elbow” above which the scatter of data points for the stars rises sharply. The distribution reaches a maximum in each case at an RMS of approximately 0.1 magnitudes. The chip and filter are labelled in the top left corner of each plot.

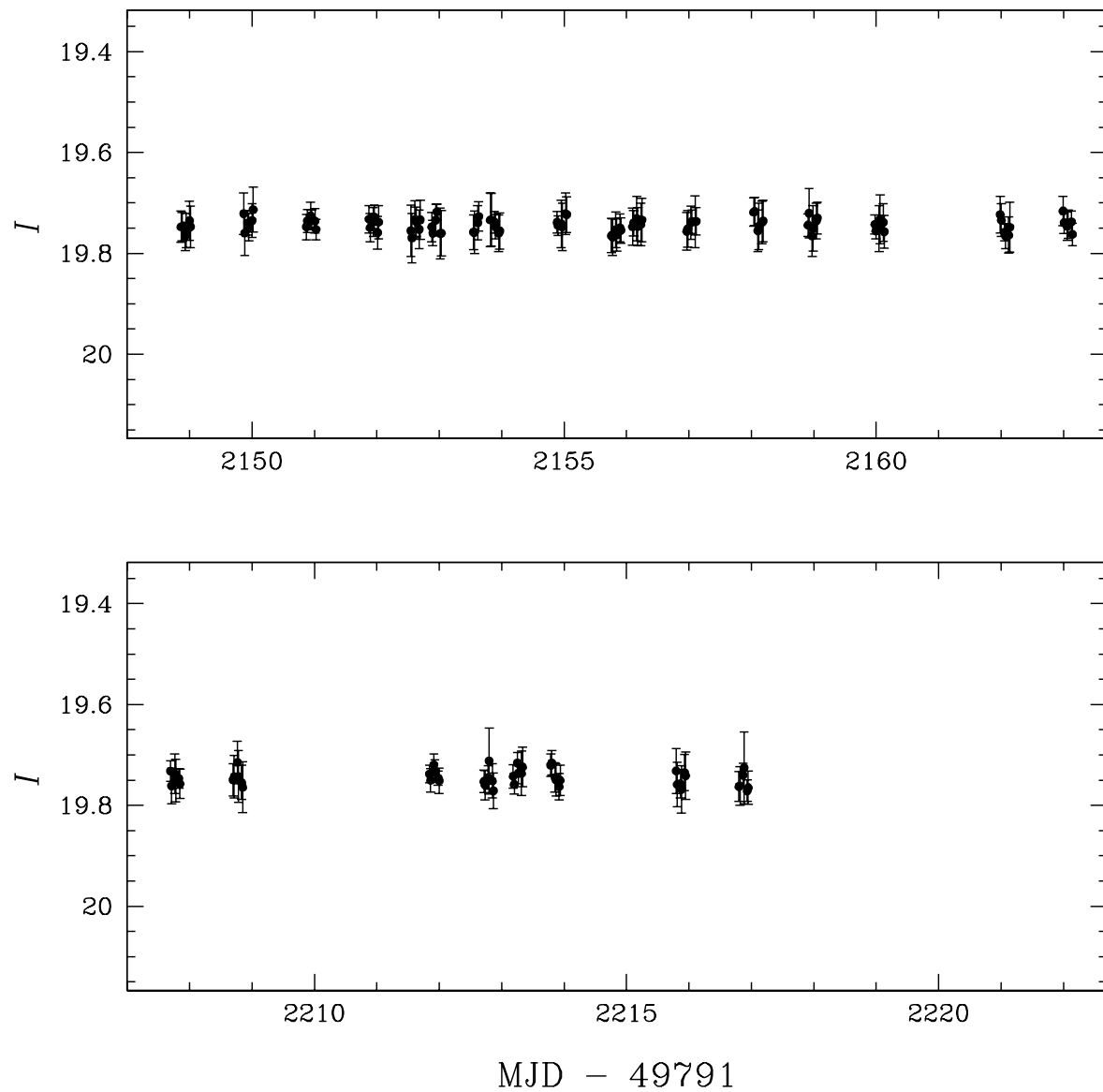


Fig. 2.— Example light curve for a star in WF4, including magnitude errors.

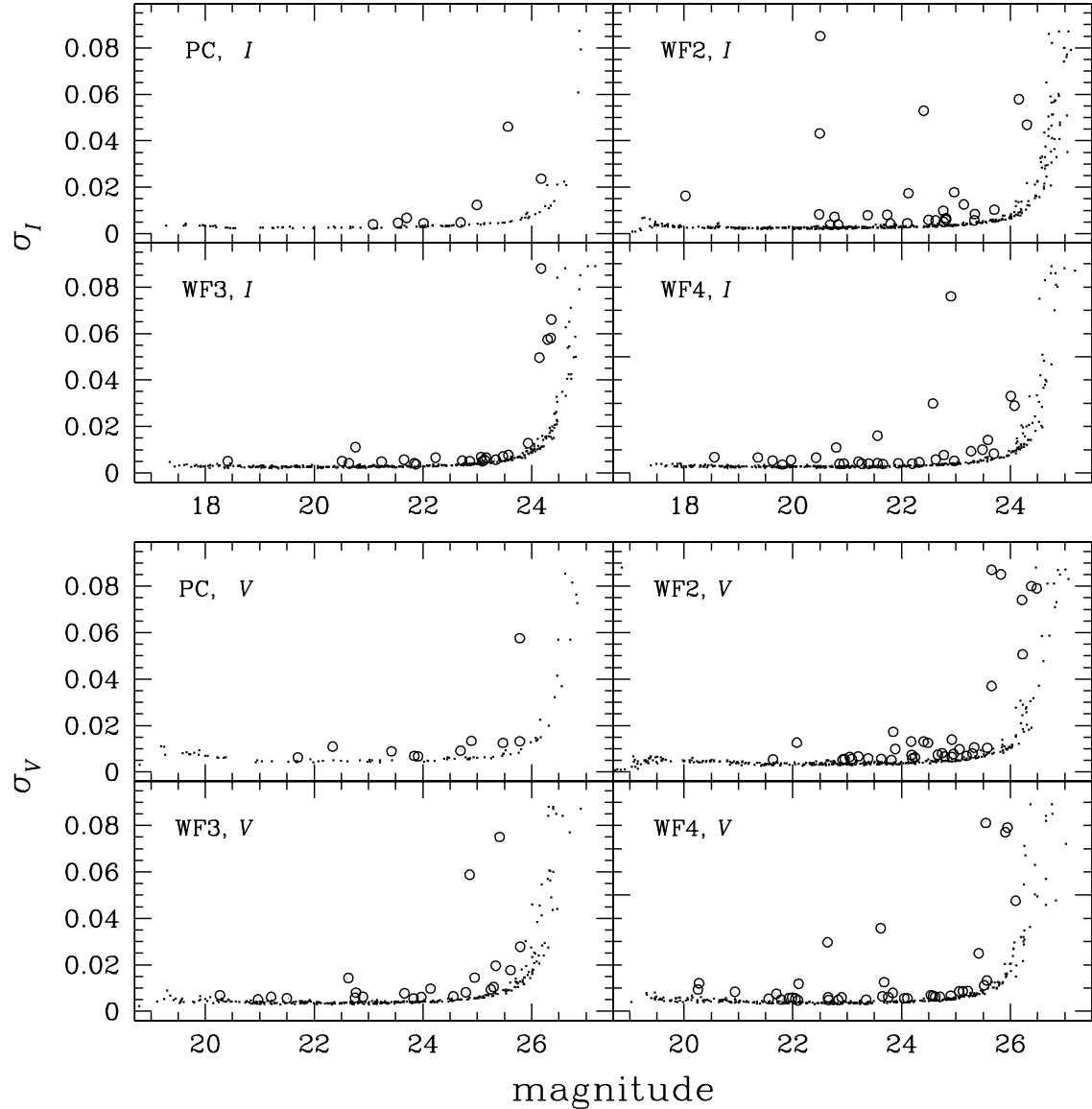


Fig. 3.— Shown again are the RMS magnitude distributions for each chip and filter. Star chosen as candidate variables are labelled as open circles.

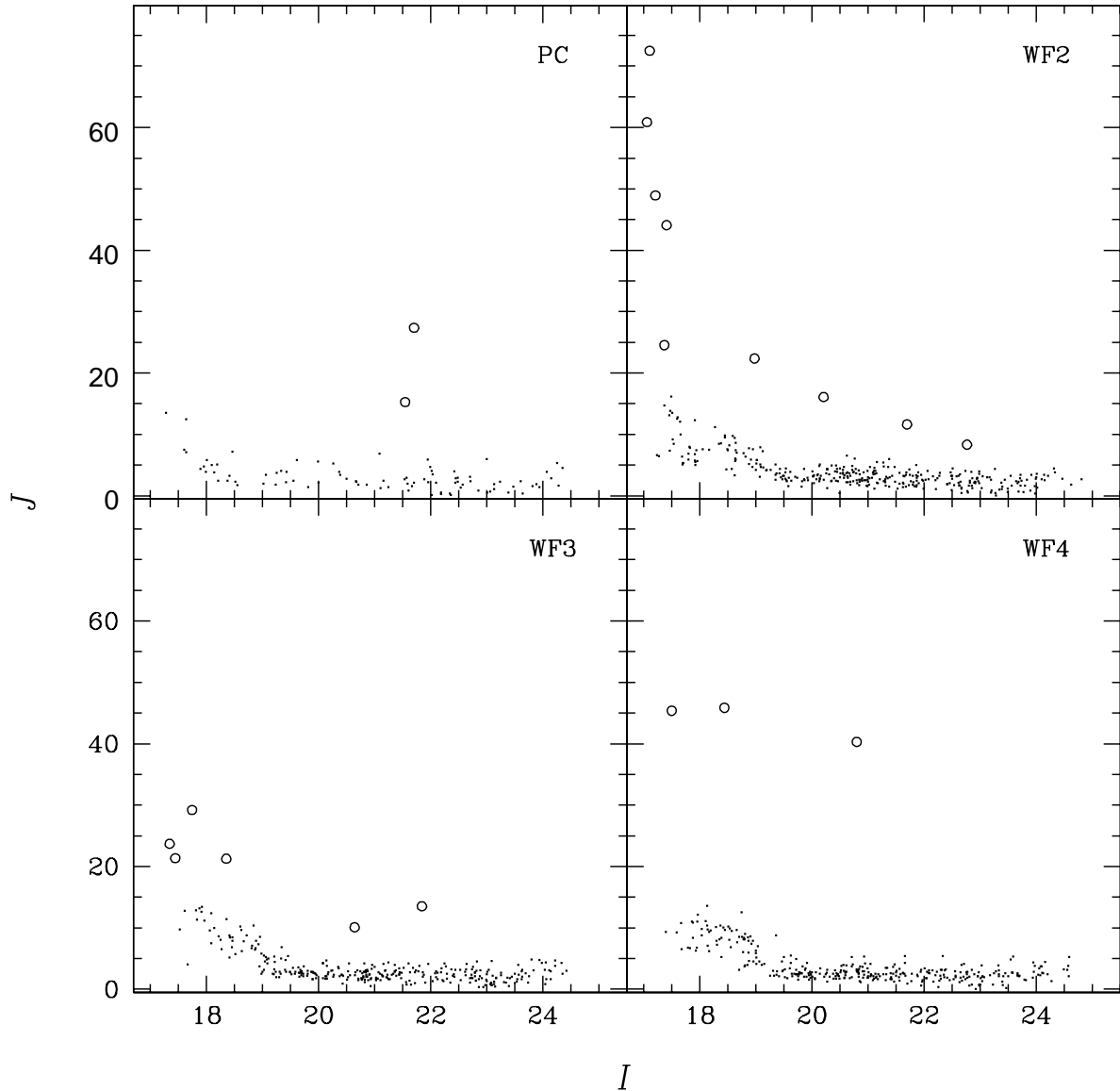


Fig. 4.— Variability index J as a function of I magnitude for stars found in each chip of WFPC2 in the M4 field. Outliers of this distribution are plotted as open circles.

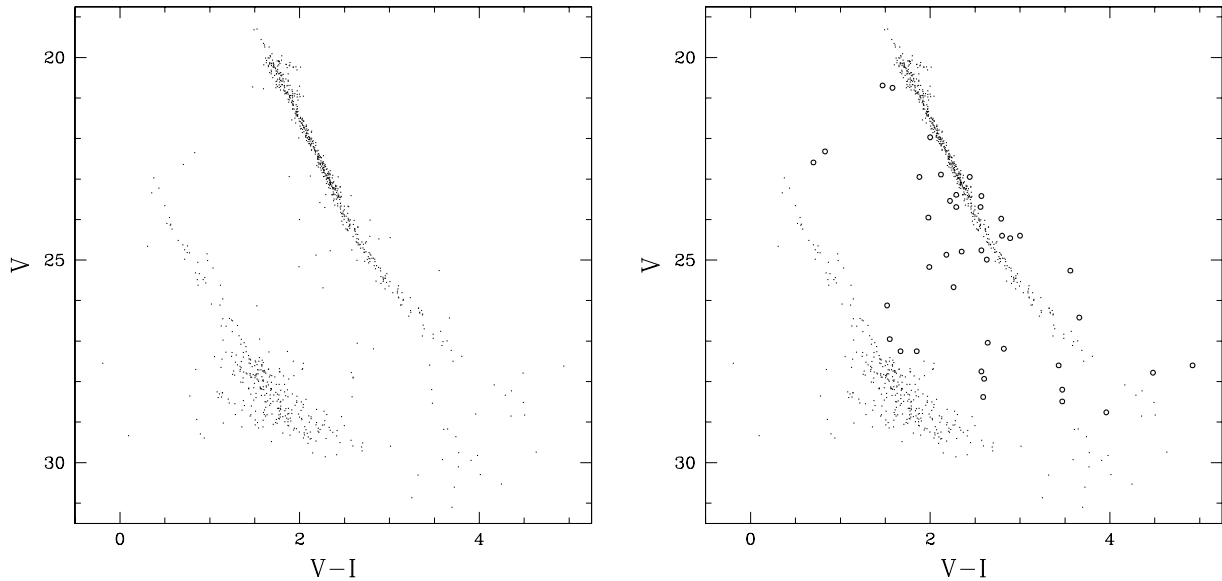


Fig. 5.— *Left*: Proper-motion cleaned color-magnitude diagram of M4. There are no signs of a binary star sequence running parallel to the main sequence of the cluster. *Right*: Main sequence and white dwarf sequence outliers chosen as variability candidates are plotted as open circles on the same CMD.

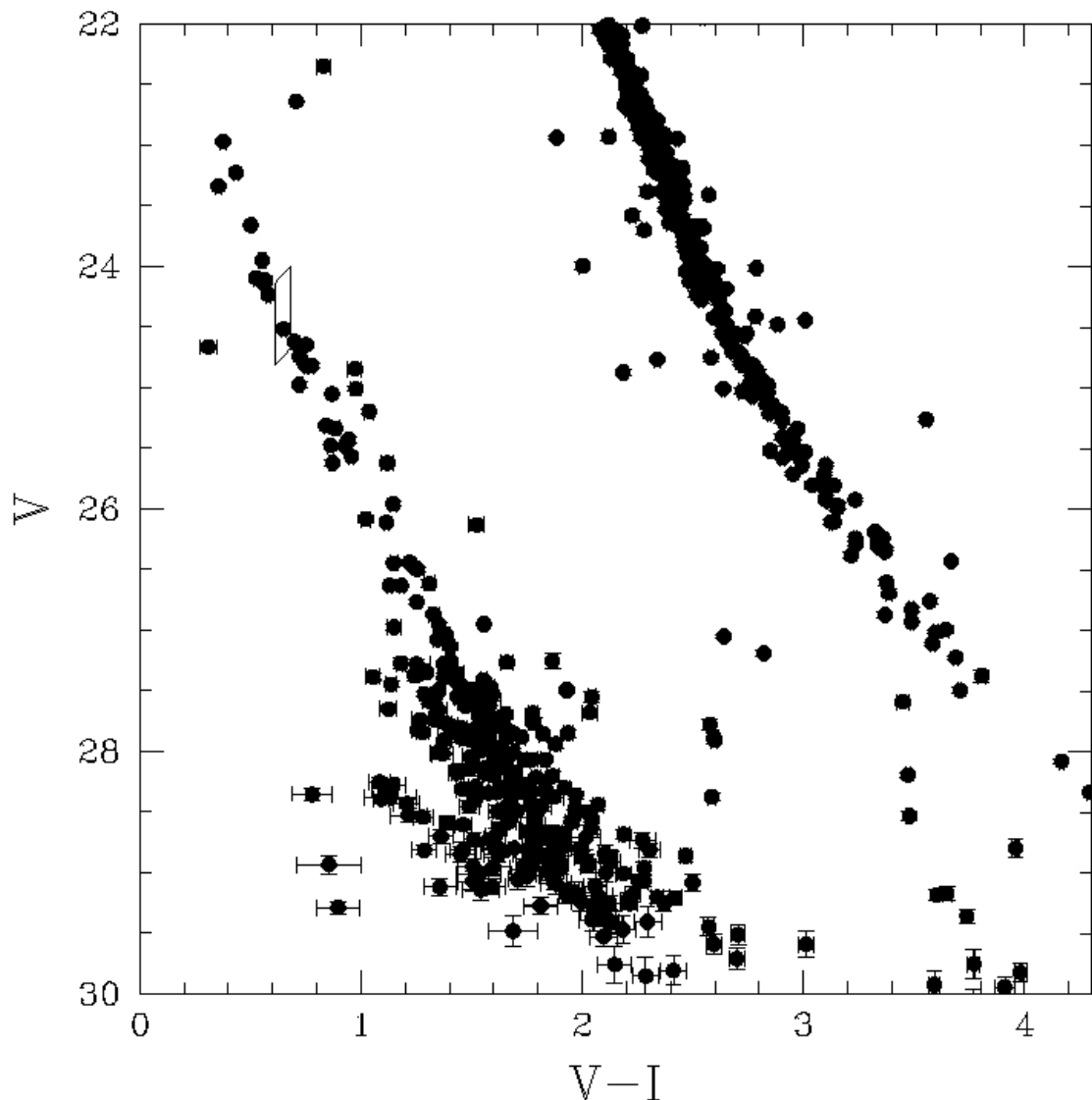


Fig. 6.— Color-magnitude diagram of M4. The ZZ Ceti instability strip through the white dwarf region is indicated by the box.

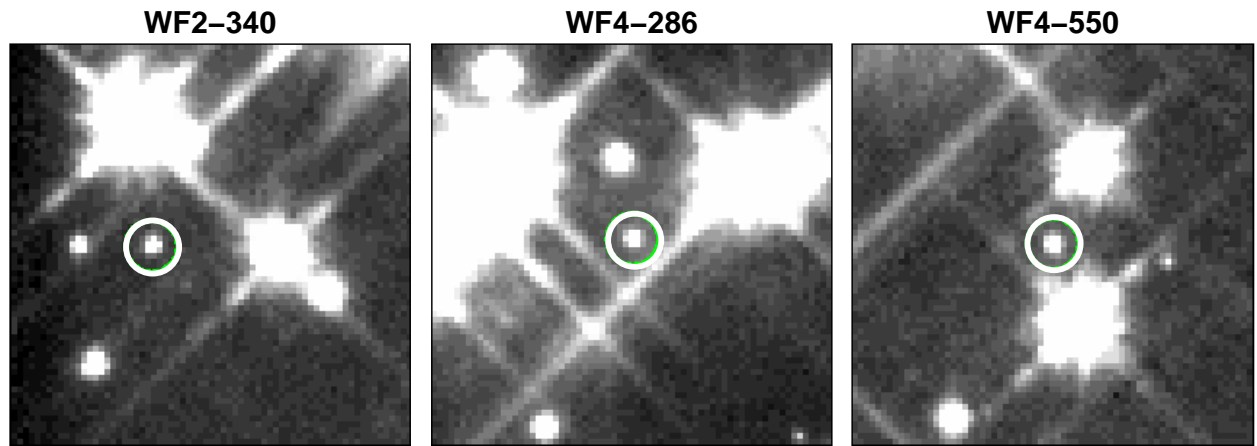


Fig. 7.— Finder charts for the candidate ZZ Ceti stars in this field. Each chart is 7×7 arcsec and the potential variables are circled.

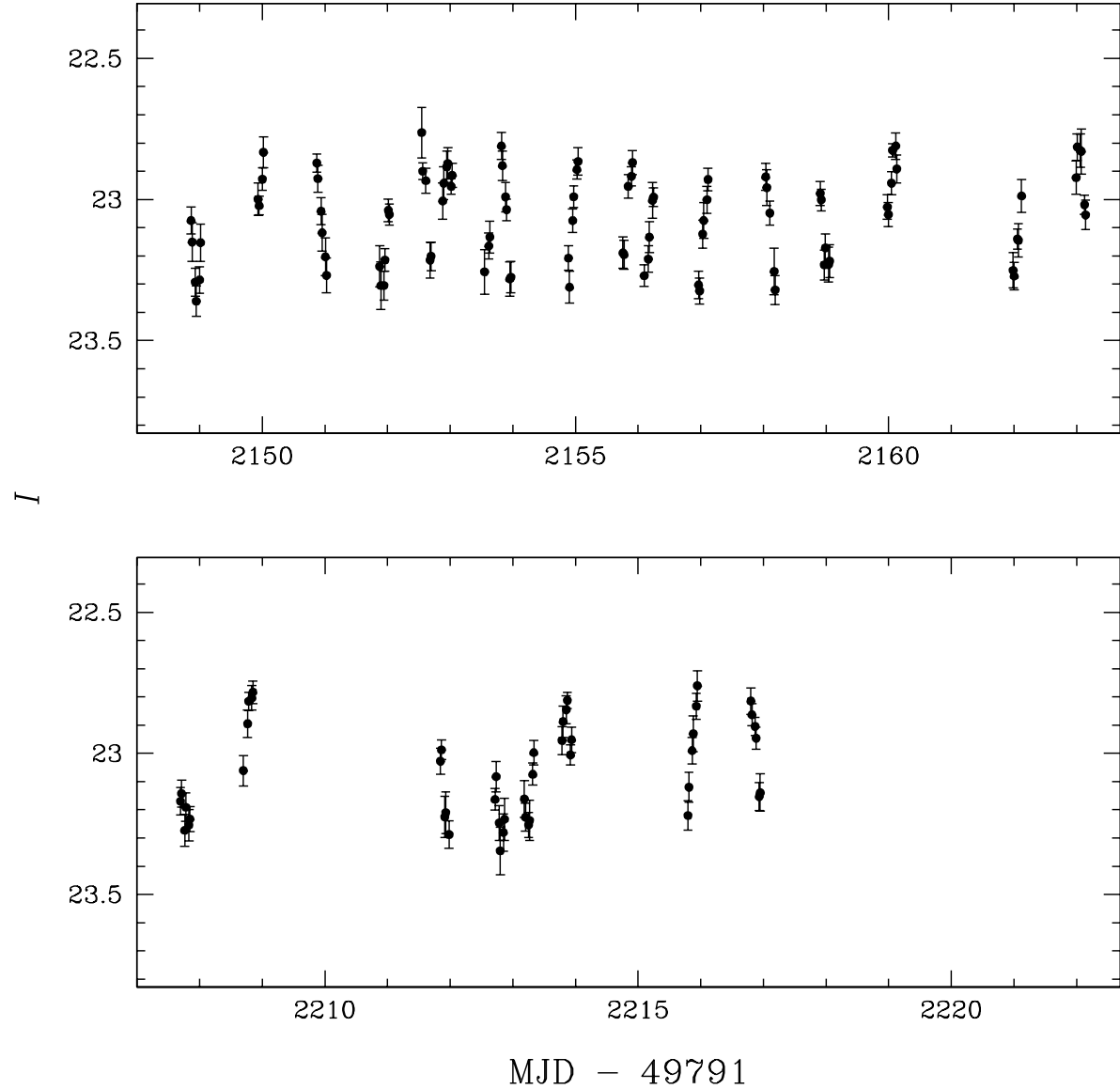


Fig. 8.— Example light curve of a sinusoid with the same time sampling as the I -band M4 data. The period is 0.42 days and the amplitude 0.2 magnitudes.

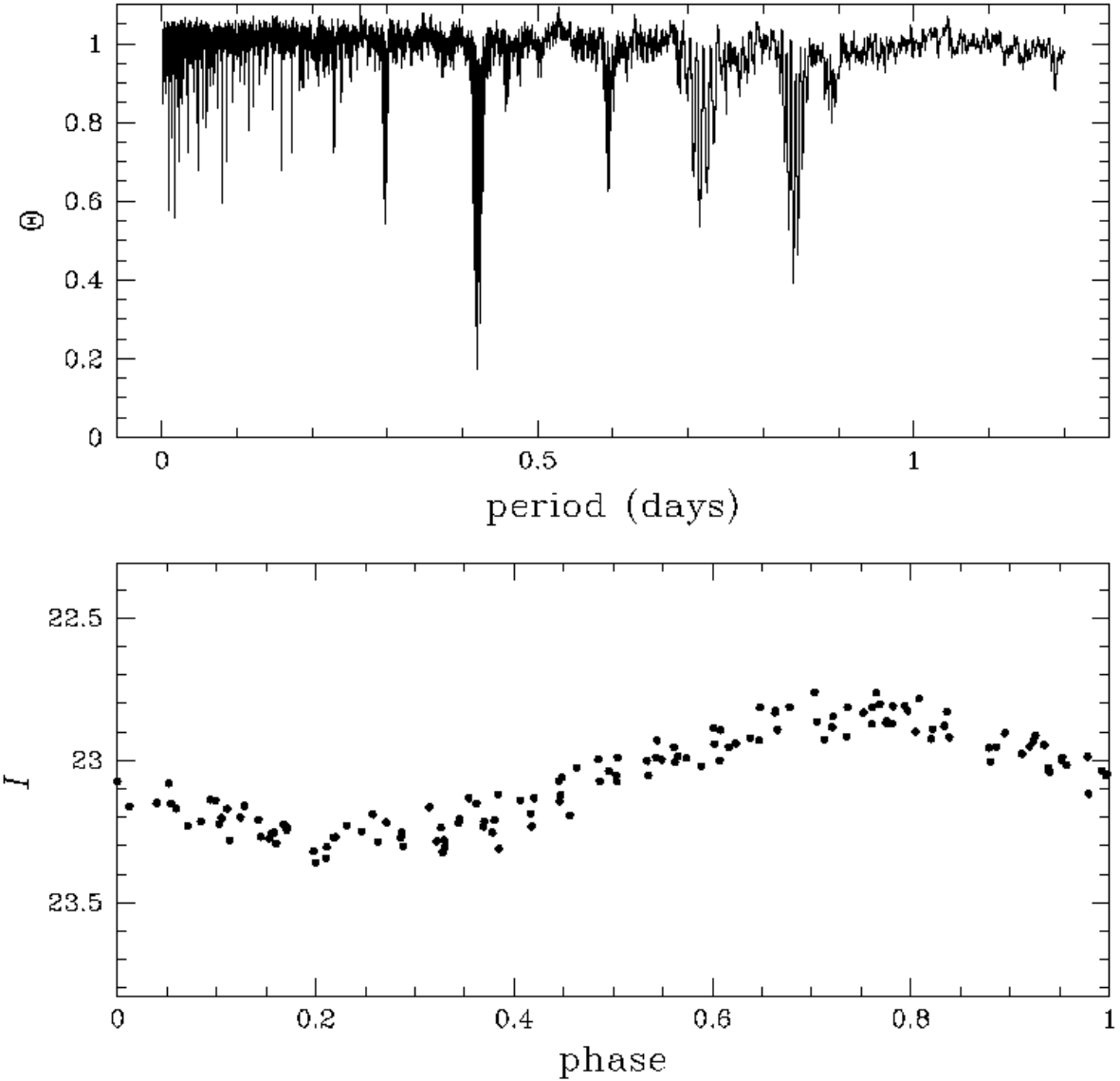


Fig. 9.— PDM analysis results of the artificial light curve shown in Figure 8. The periodogram (above) shows that the analysis finds the correct period for that light curve. Below is the light curve folded into the period associated with the lowest value of Θ , 0.42 days.

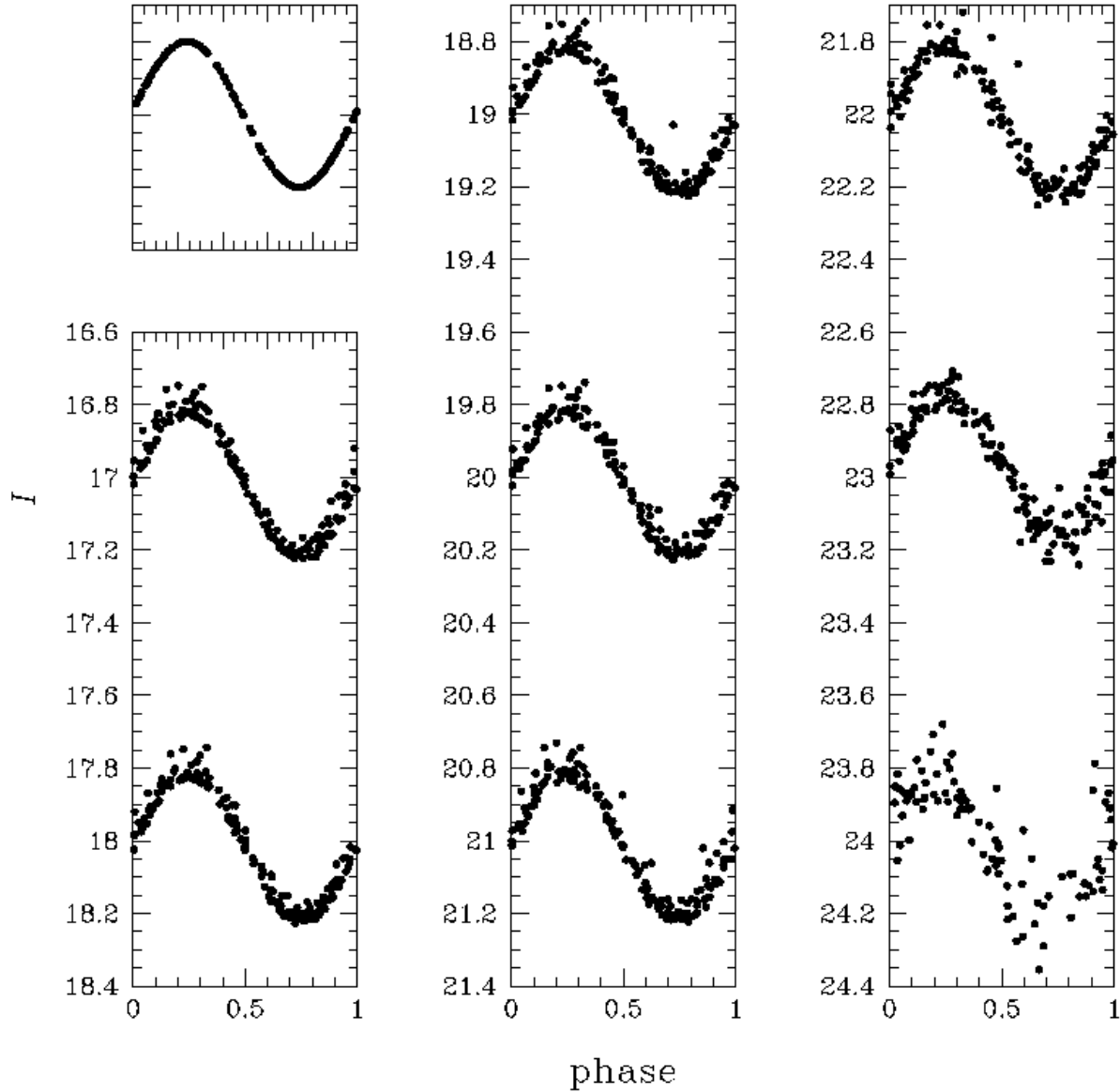


Fig. 10.— Artificial sinusoidal light curves, The curves are phase folded to their input period of 0.42 days. The curve on the top left is without noise, and is plotted on the same scale as the rest shown. Note the increase in noise levels and scatter of the curves at fainter magnitudes.

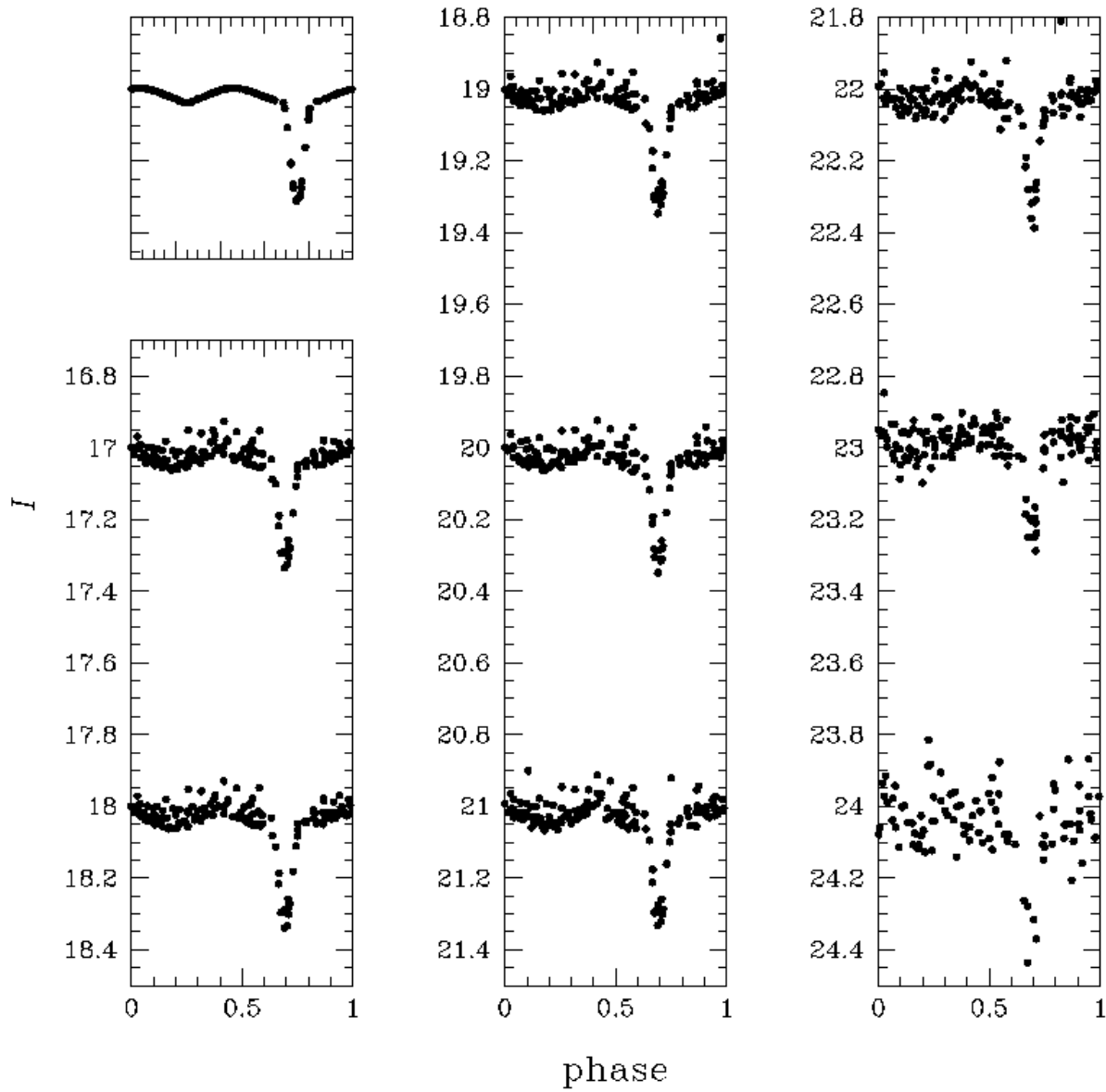


Fig. 11.— Artificial Algol-type light curves with period 0.42 days, presented as in Figure 10.

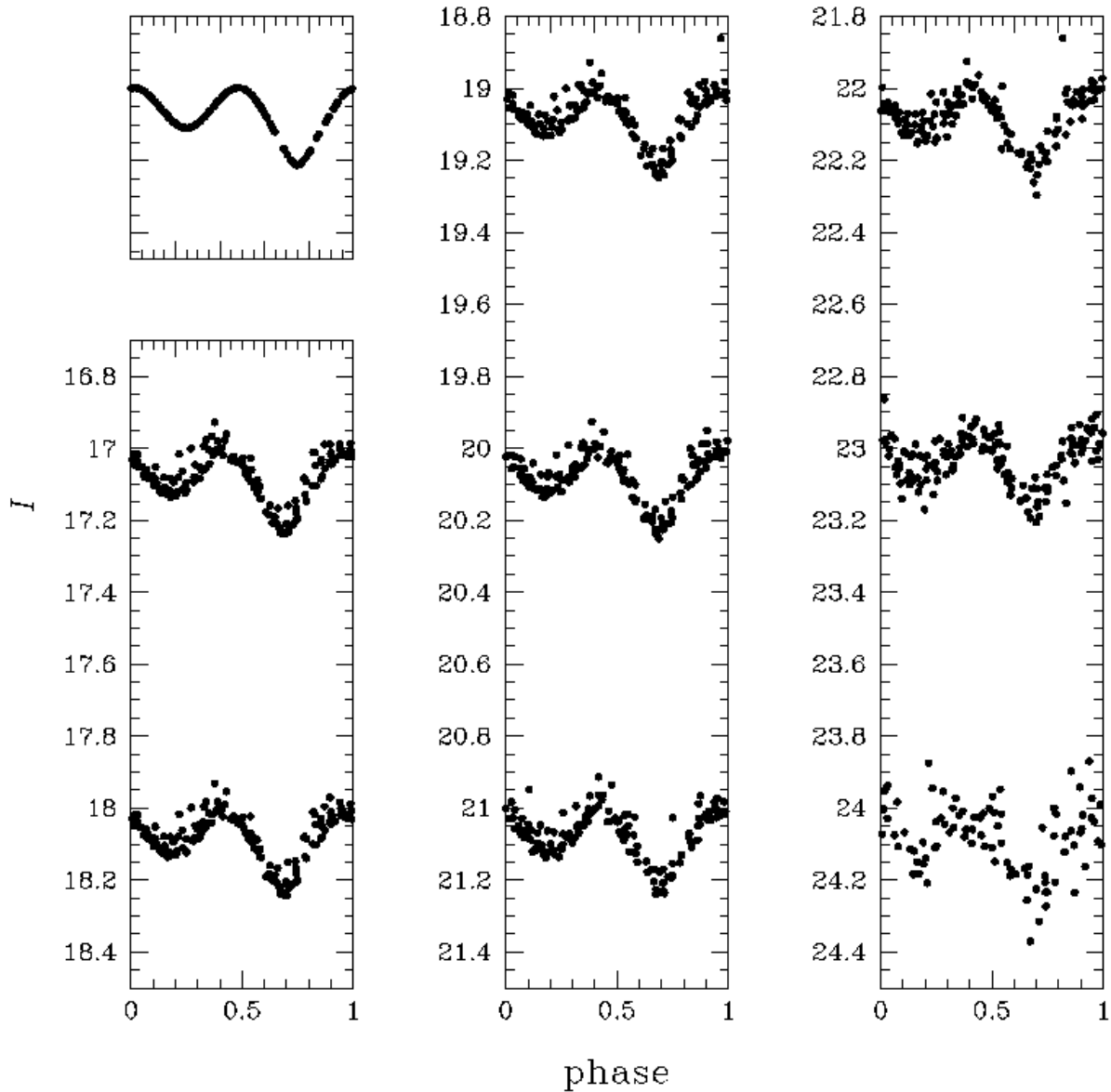


Fig. 12.— Artificial W UMa-type light curves with period 0.42 days, presented as in Figure 11.

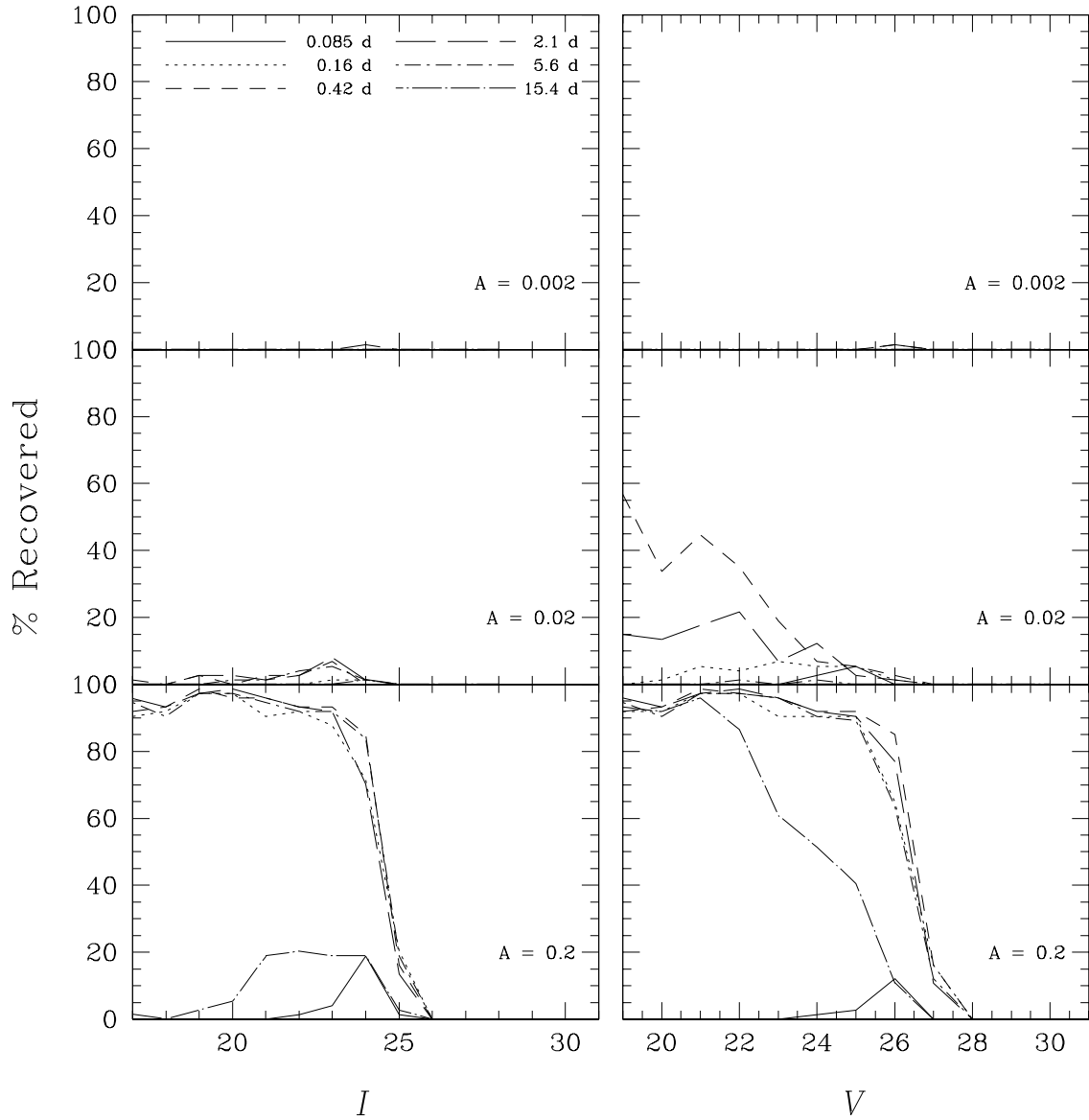


Fig. 13.— Results of PDM analysis on an artificial sinusoidal light curve for a range of periods and amplitudes. A successful recovery is considered to be within 1% of the input period.

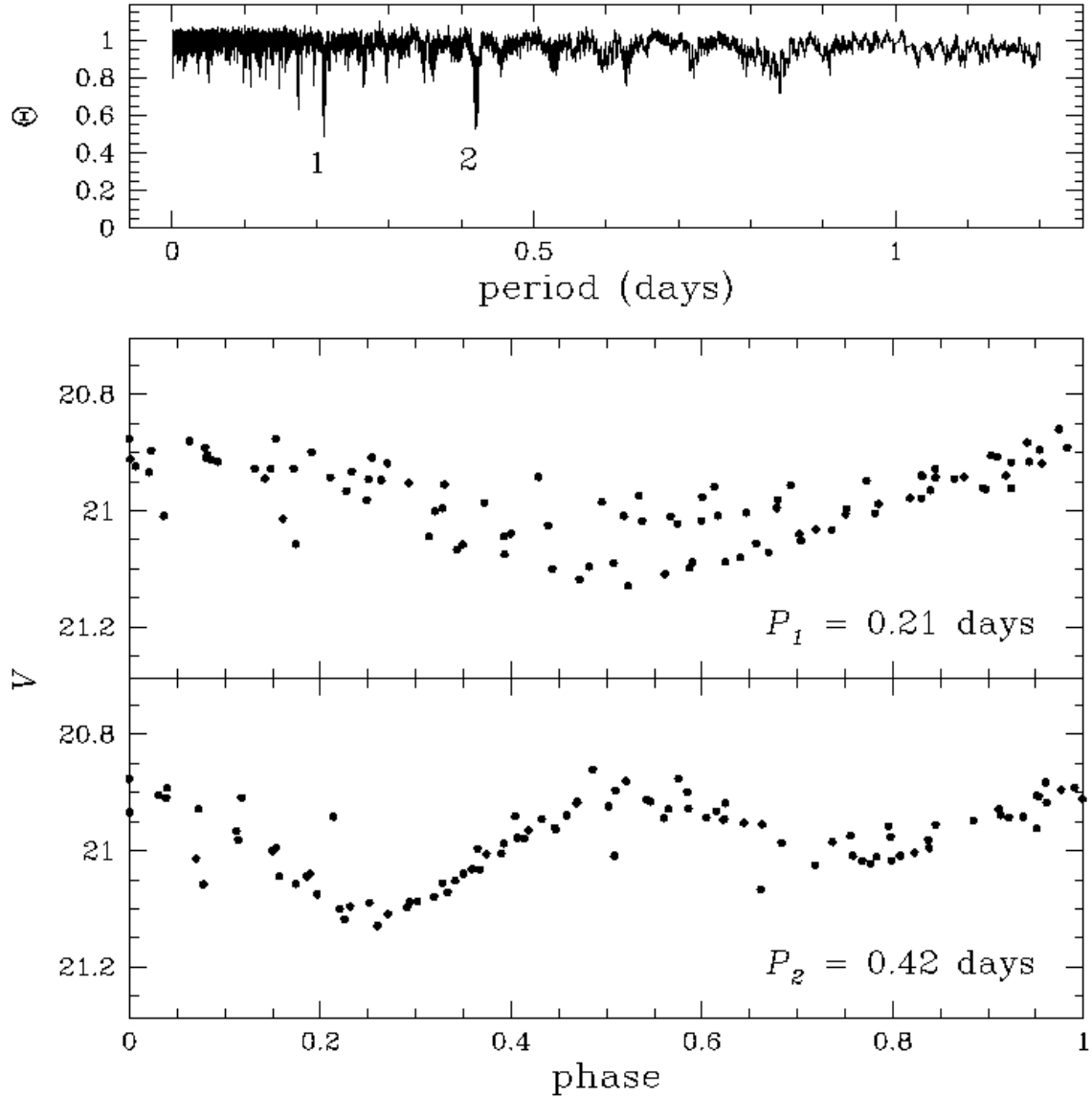


Fig. 14.— Results of PDM analysis on an artificial W UMa-type light curve. *Top*: The period corresponding to the lowest value of Θ is 0.21 days (1). This is half the input period, which has a corresponding Θ value which is only slightly greater (2). *Bottom*: Phase-folded light curves corresponding to 0.21 and 0.42 day periods. The lower Θ value for the 0.21 day period is probably due to the size of bins used in evaluating the total variance of the phase-folded light curve.

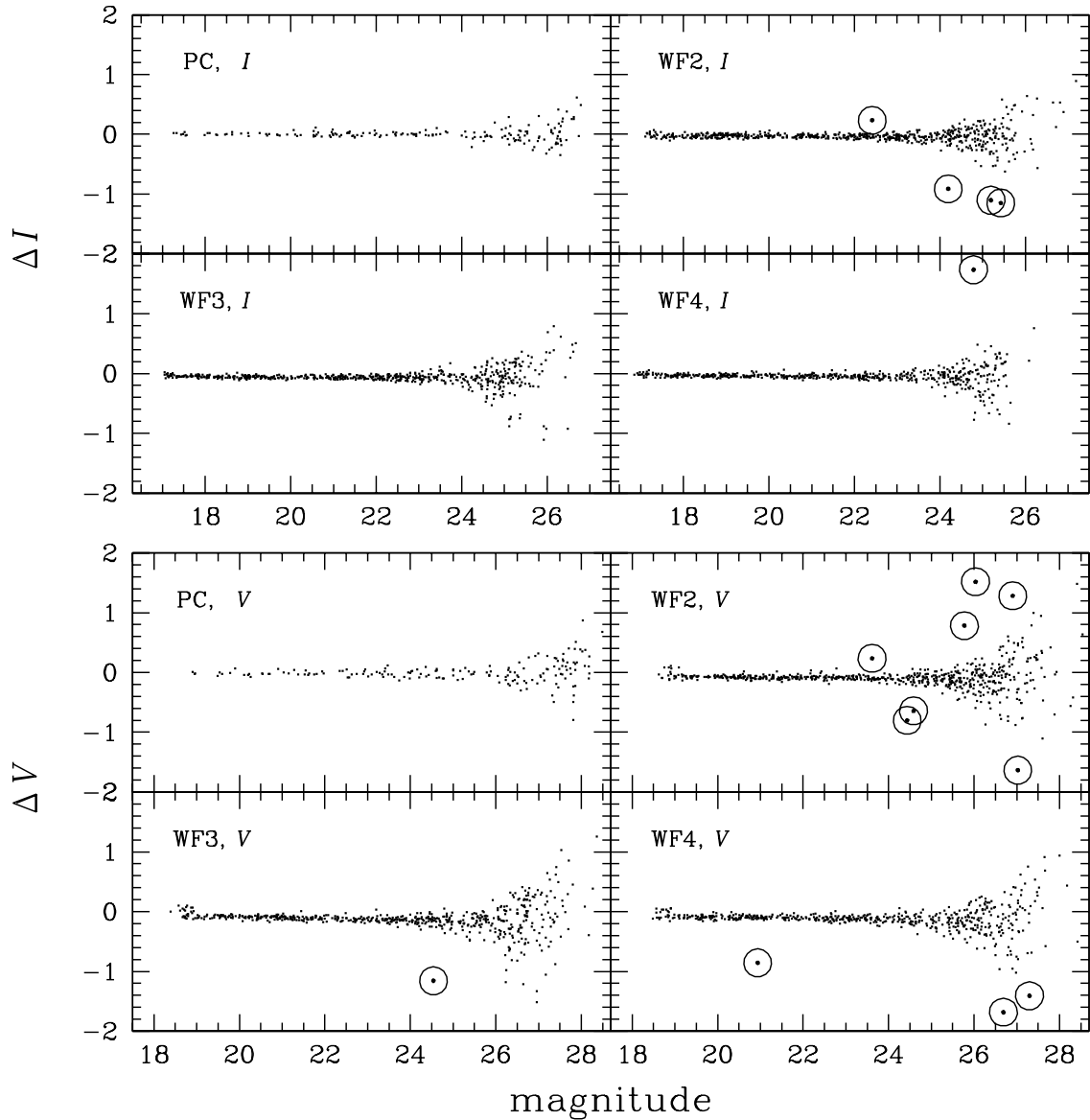


Fig. 15.— Distribution of magnitude differences between the epoch 1 and epoch 2 combined images. Outliers to this distribution were chosen as candidate supernovae and are marked by open circles.

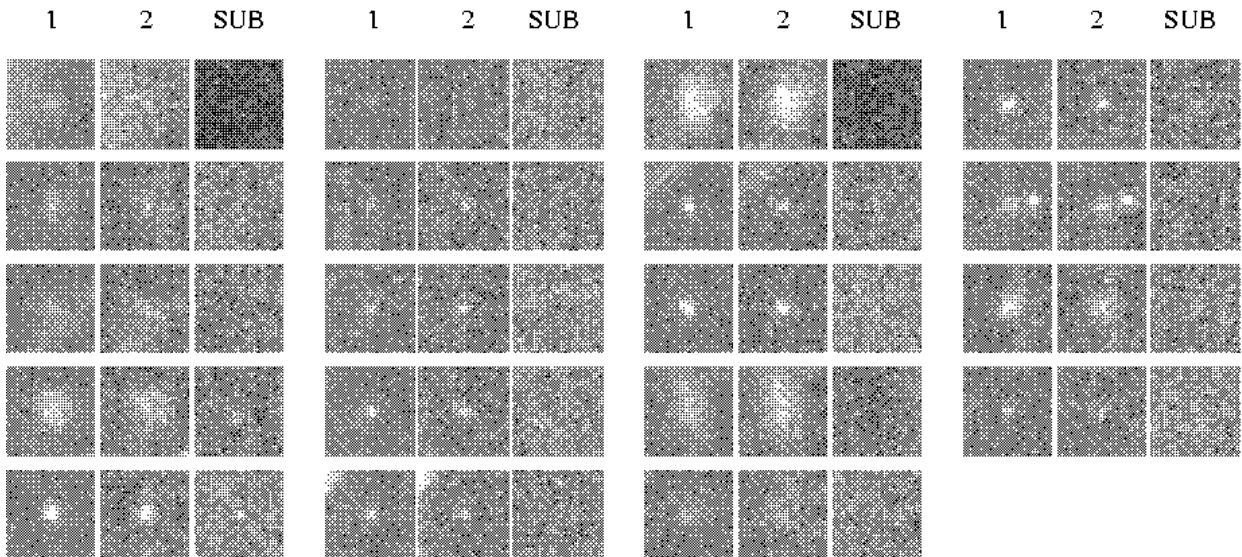


Fig. 16.— Results of image subtraction performed on the PC chip I -band data. Shown are 20×20 pixel subsets of the full image, each one centered on the coordinates of the galaxies found on the image. These images are organized into three columns: the epoch 1 combined image, the epoch 2 image, and the (epoch 1 – epoch 2) image. The resulting subtracted image showed no signs of residual flux $\gtrsim 1\sigma$ above or below the mean noise level (A high-resolution version of this image can be found at <http://www.astro.ubc.ca/~ferdman>).

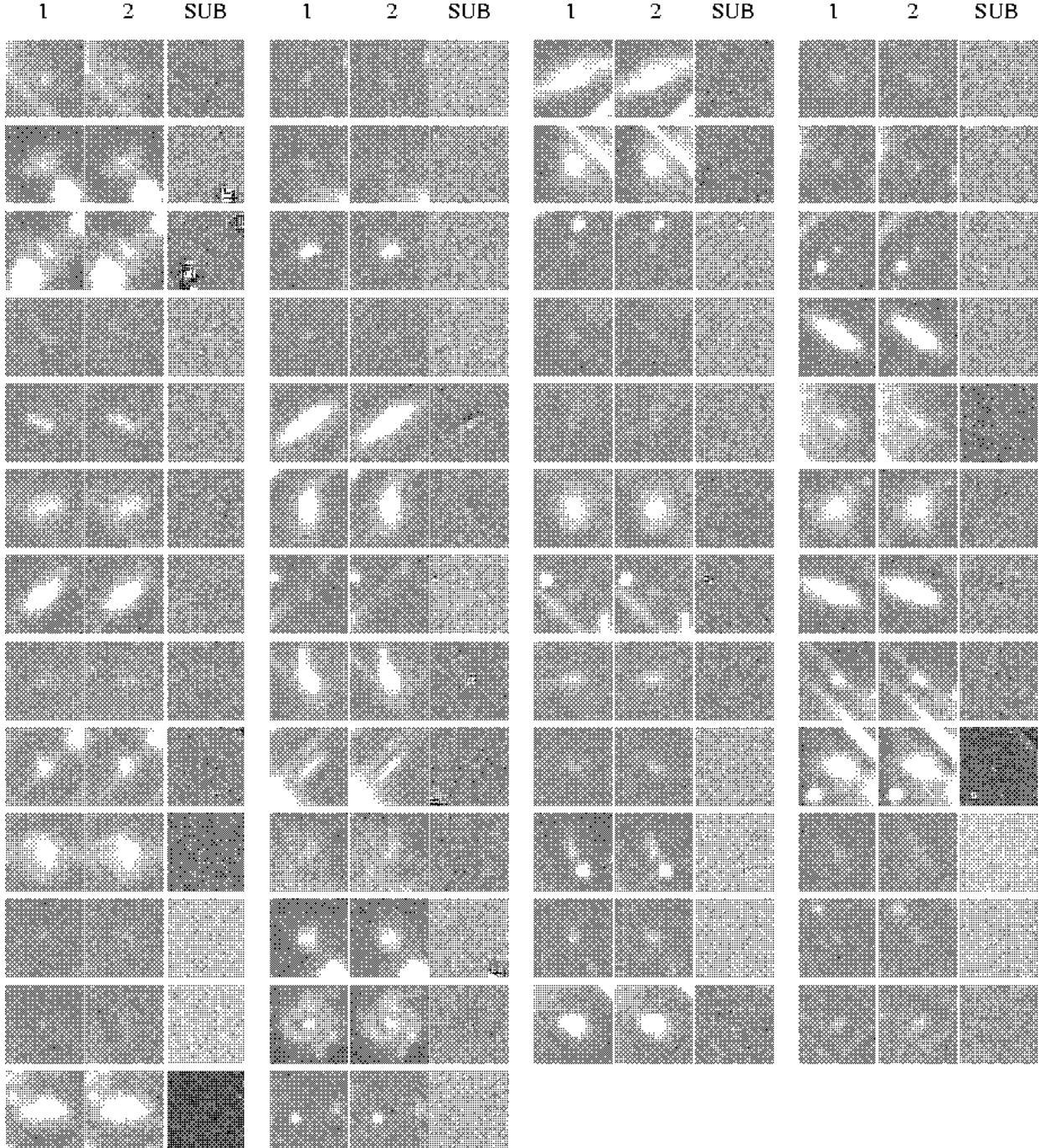


Fig. 17.— Results of image subtraction performed on the WF2 chip I -band data. Shown are 30×30 pixel subsets of the full image, presented as in Figure 16 (A high-resolution version of this image can be found at <http://www.astro.ubc.ca/~ferdman>).

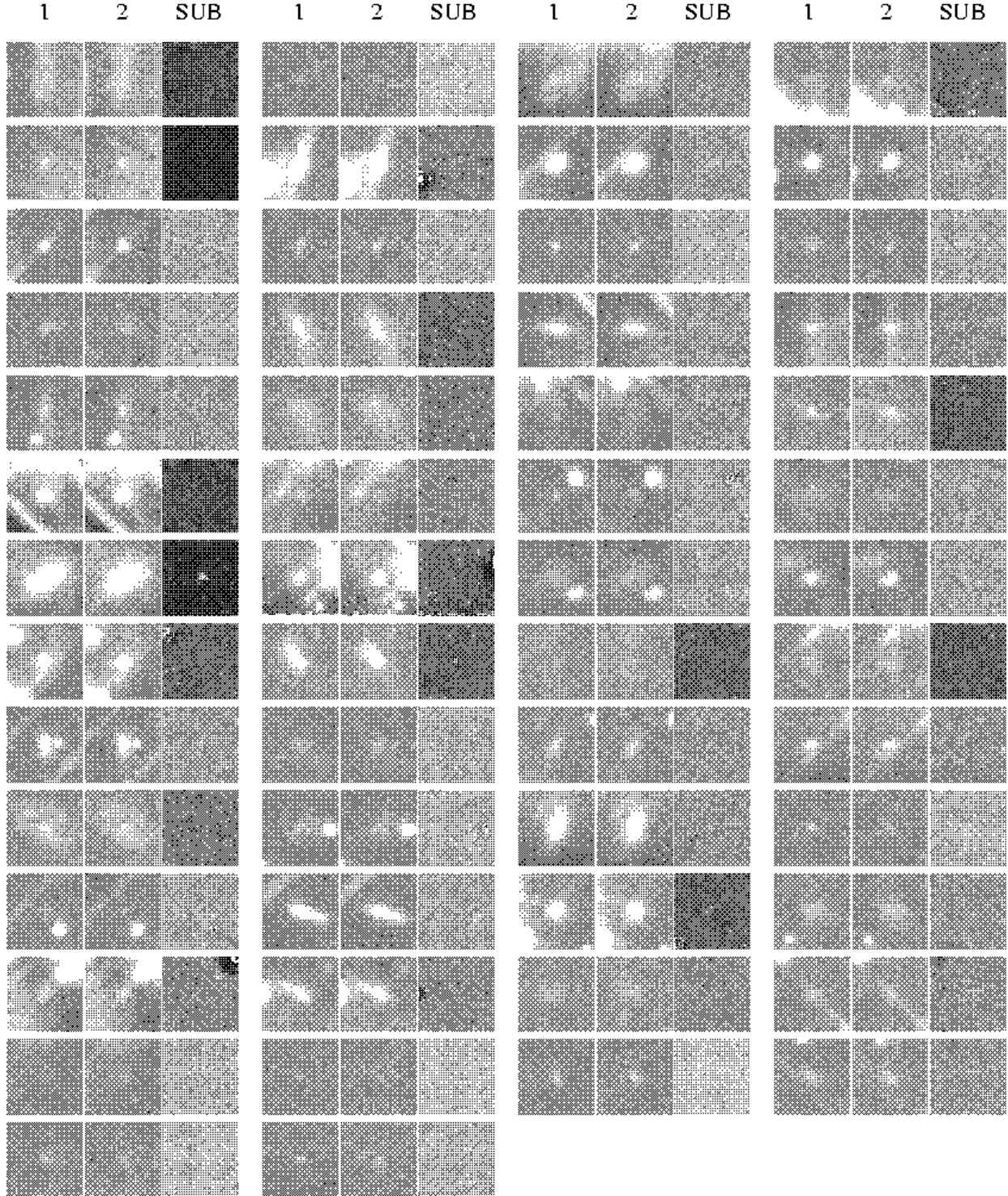


Fig. 18.— Results of image subtraction performed on the WF3 chip *I*-band data. Shown are 30 × 30 pixel subsets of the full image, presented as in Figure 16 (A high-resolution version of this image can be found at <http://www.astro.ubc.ca/~ferdman>).

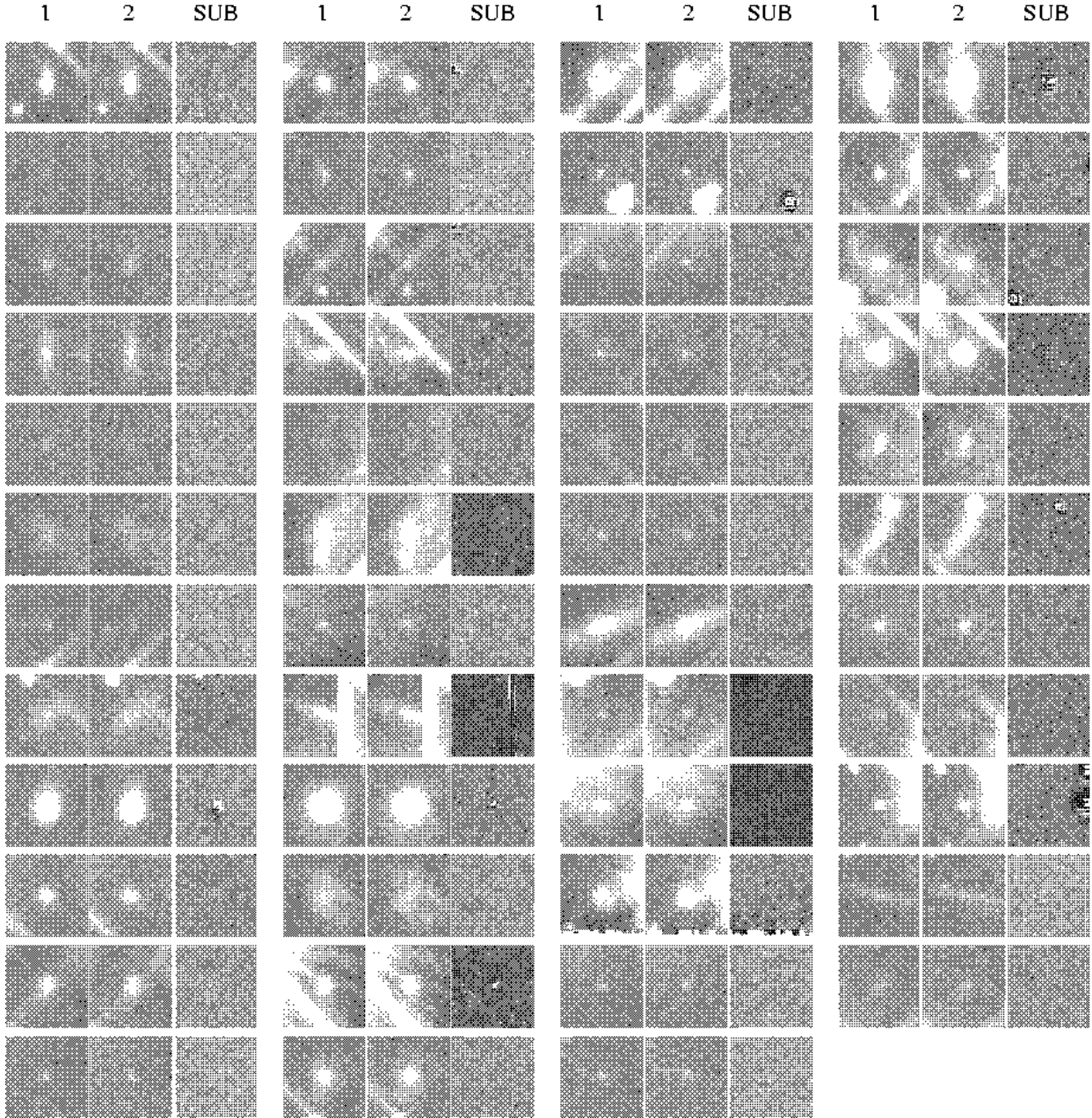


Fig. 19.— Results of image subtraction performed on the WF4 chip *I*-band data. Shown are 30×30 pixel subsets of the full image, presented as in Figure 16 (A high-resolution version of this image can be found at <http://www.astro.ubc.ca/~ferdman>).

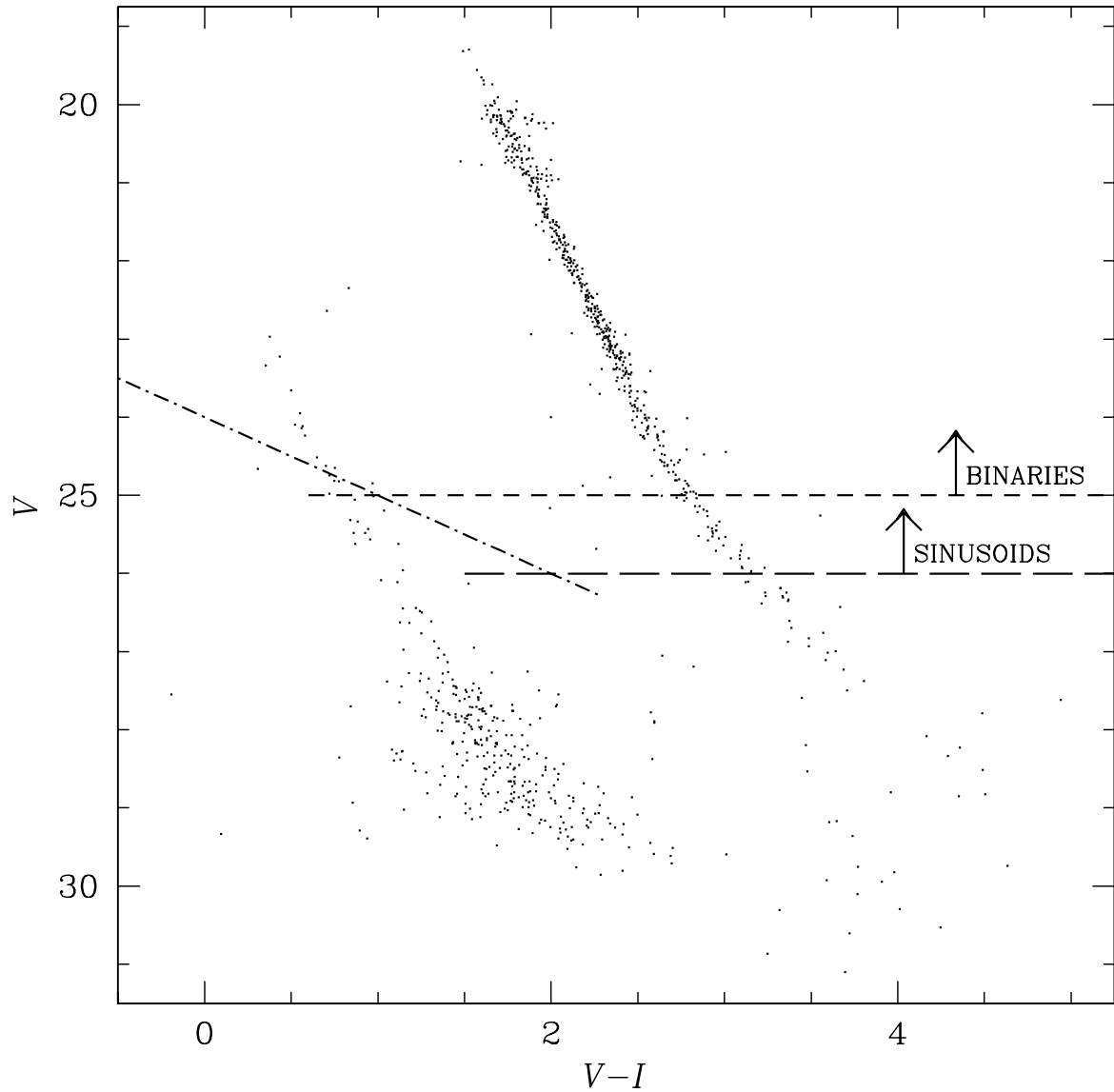


Fig. 20.— The same color-magnitude diagram as in Figure 5, with the limiting magnitudes shown as intersecting dashed lines, above which PDM analysis was successful in recovering input periods for artificial binary star (upper dashed line) and sinusoidal-type (lower dashed line) light curves.

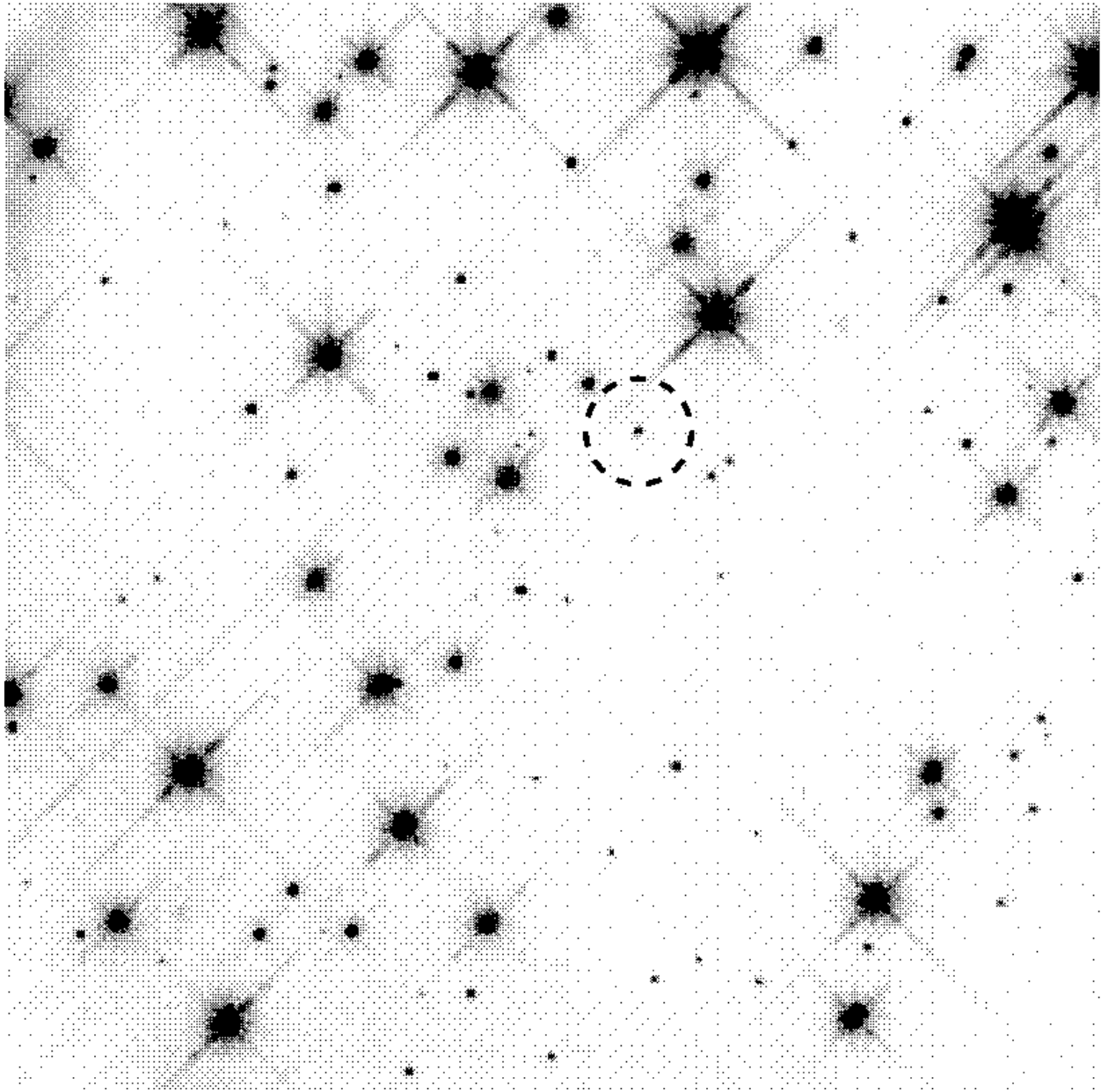


Fig. 21.— The combined *I*-band PC chip image of the M4 field taken with *HST*. The remaining candidate from the variable star search is enclosed by a dashed circle. It is a relatively isolated star, in that it is not close to a saturated star or a diffraction spike. It is also very far from the edge of the image (A high-resolution version of this image can be found at <http://www.astro.ubc.ca/~ferdman>).

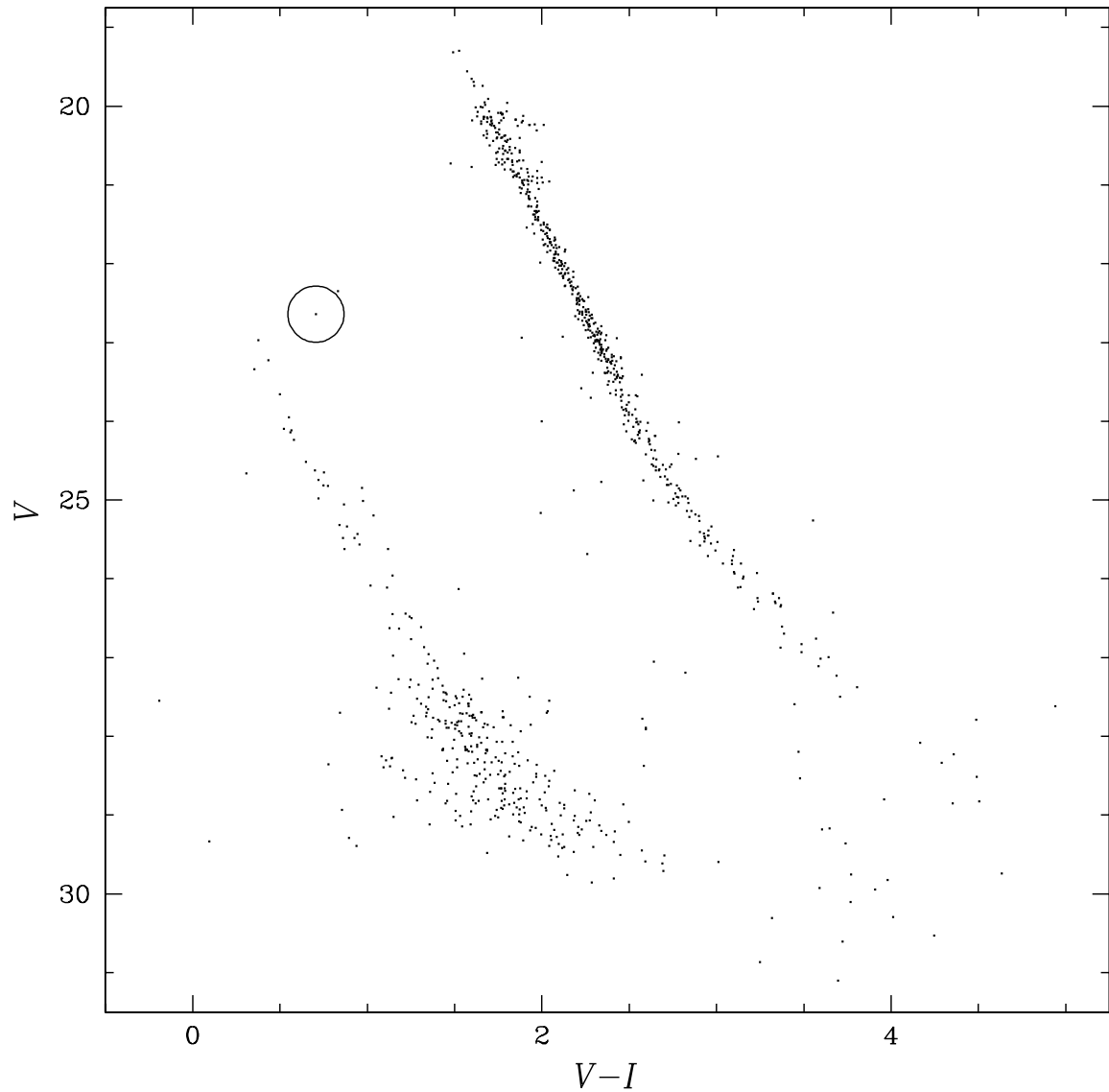


Fig. 22.— The same CMD of M4 shown in Figure 5, with the remaining candidate star circled. It is at the bright end and slightly to the red of the white dwarf sequence of the cluster. The object just to the red and slightly more luminous was found very close to the edge of the image, and was found to disappear from and reappear in the image over time, and was excluded from being a candidate variable.

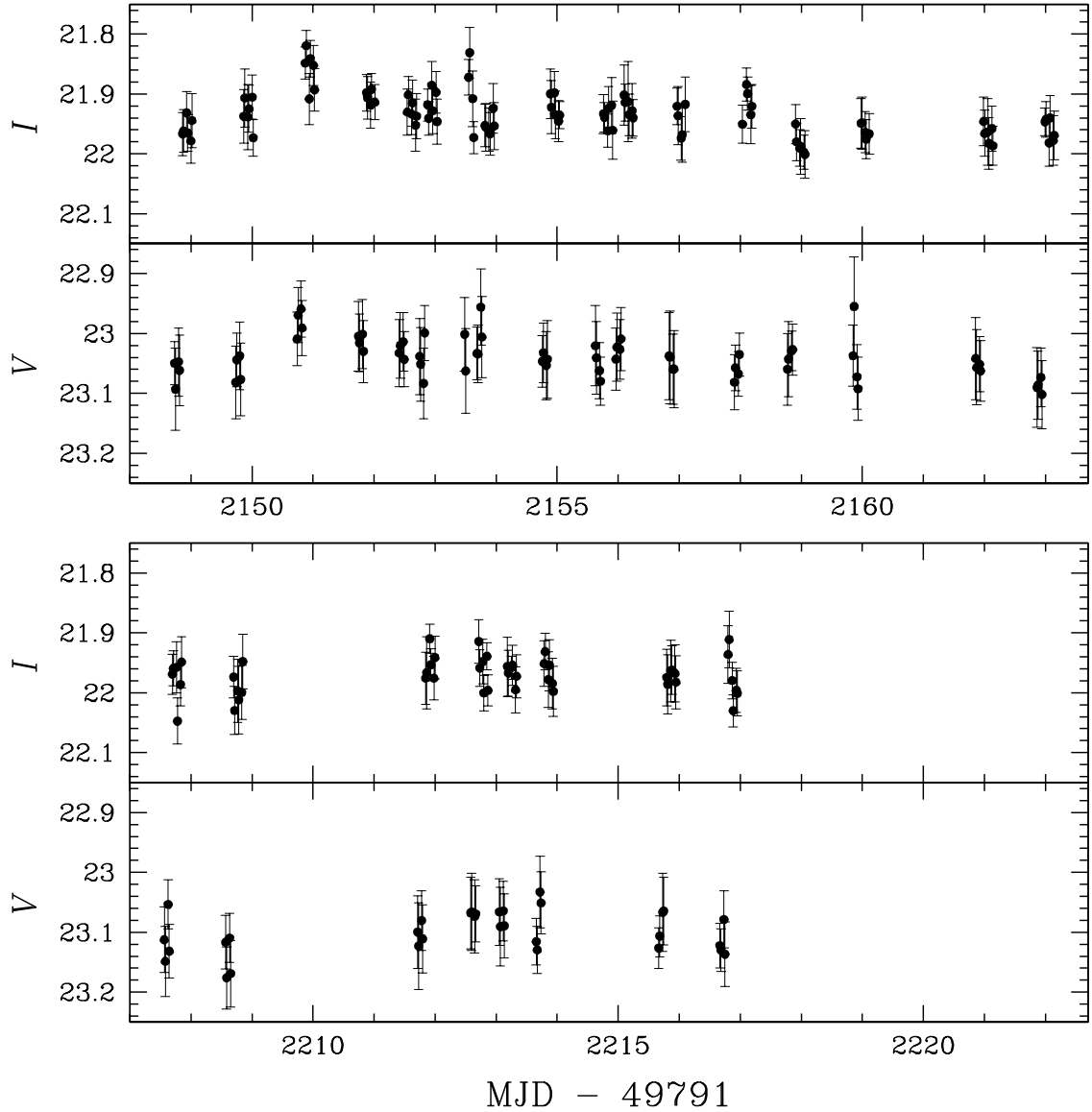


Fig. 23.— Light curve of the remaining candidate variable star. The first set of rows shows the light curve before the 45 day gap in the observations, and the second set shows the light curve after that gap. It can be seen that the light curve shows a ~ 0.1 magnitude rise in its amplitude a few days into the observations in both the I and V filter data, which is a highly desirable characteristic in the selection of this star as a candidate.

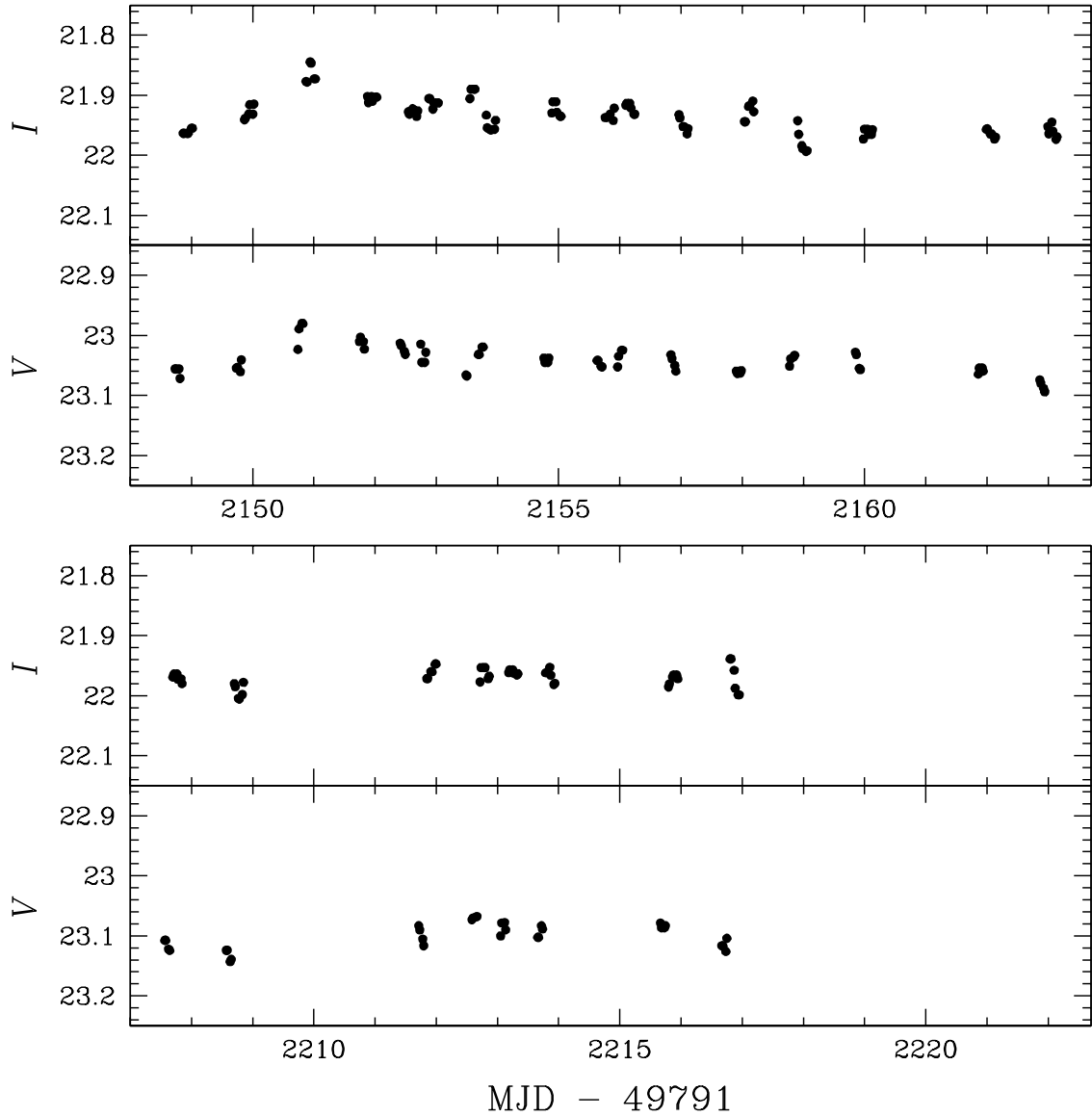


Fig. 24.— Median-smoothed light curve of the remaining candidate variable star. The ~ 0.1 magnitude rise in its amplitude a few days into the observations in both the *I* and *V* filter data is more prominent here than in the un-smoothed light curve shown in Figure 23.

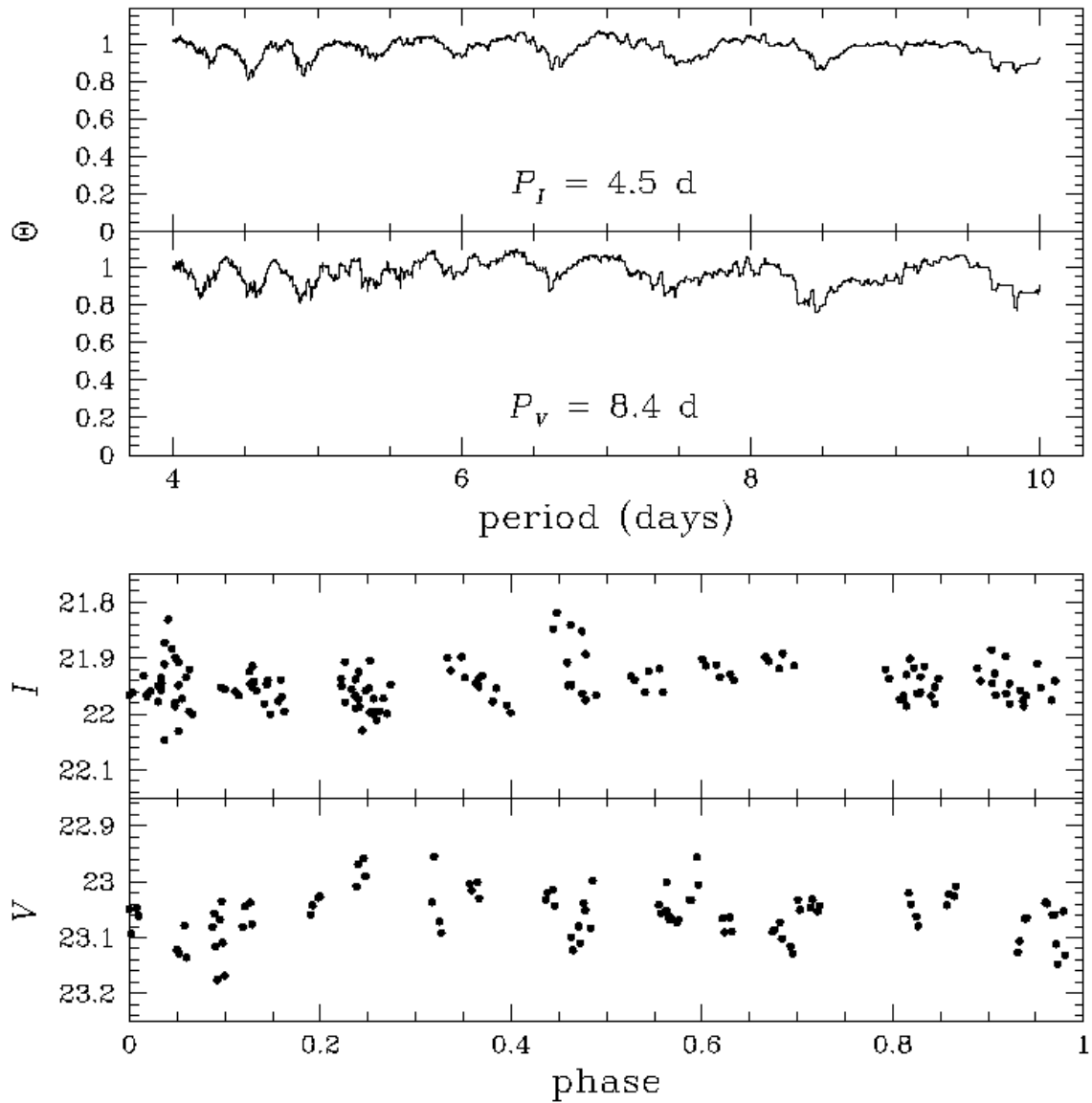


Fig. 25.— Results of phase dispersion minimization analysis of the remaining candidate variable star. *Top*: Θ distribution periodograms for observations in each bandpass. Although there is no significant deviation of Θ from a value of 1, the features of the periodogram are very similar between the two sets of data. *Bottom*: Phased light curves, folded into the period associated with the lowest found values of Θ .

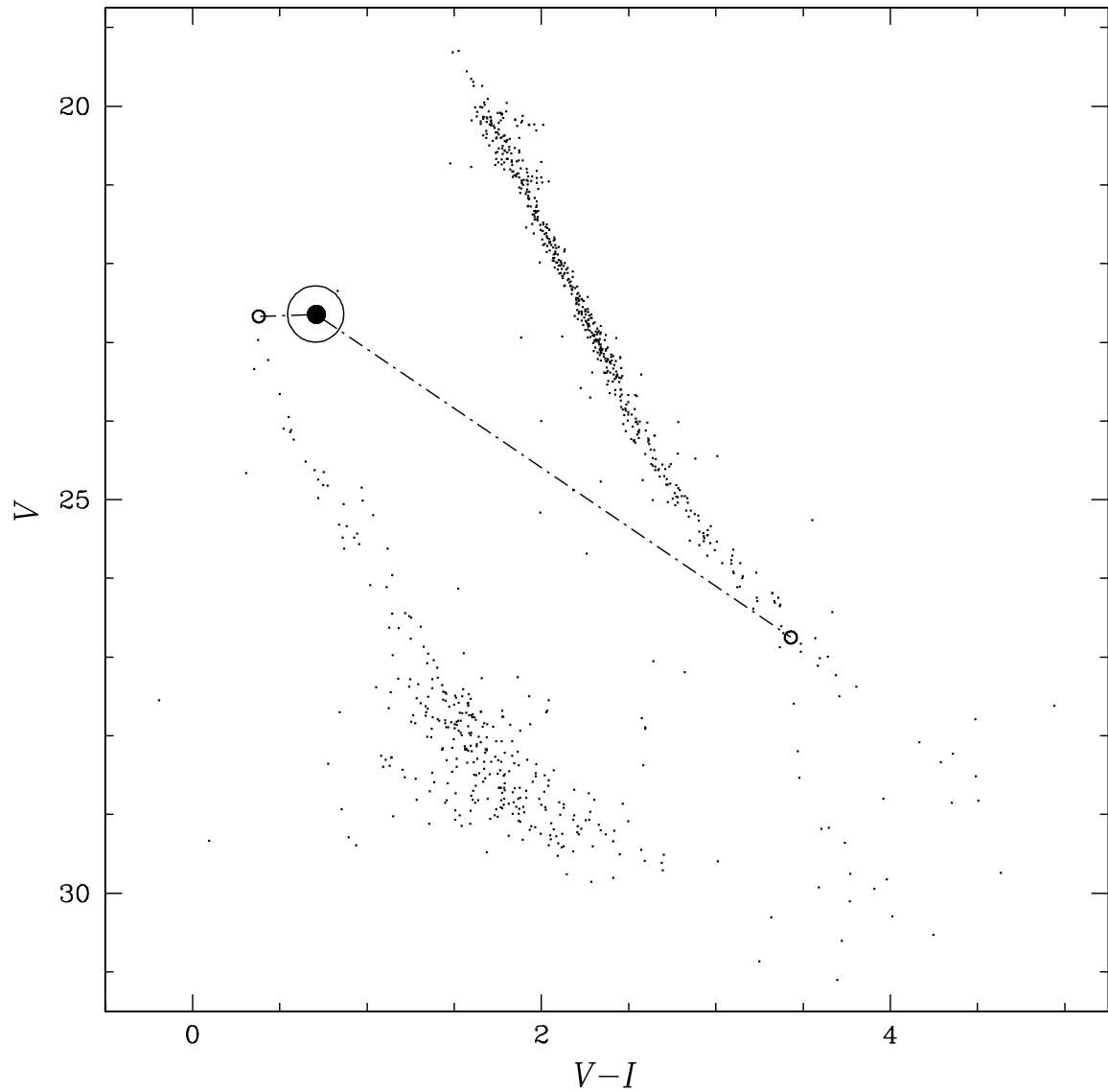


Fig. 26.— Color-magnitude diagram of M4 showing the positions of the two stars (smaller open circles) needed to produce a binary system that would be observed with similar magnitude and color as the candidate star (filled circle). The resulting object is very close in position to the candidate, which is located at the center of the large open circle.

Table 1. RMS outlier candidates for variability search.

Chip	ID	RA ^a	Dec ^a	Filters ^b	<i>V</i>	σ_V	$V - I$	σ_{V-I}	Comments
PC	1	16:23:56.26	-26:32:27.0	<i>I, V</i>	22.349	0.024	0.831	0.042	isolated; very near to edge of image
PC	2	16:23:55.28	-26:32:35.8	<i>I, V</i>	23.383	0.017	2.360	0.020	isolated; close to edge of image
PC	3	16:23:54.59	-26:32:42.2	<i>I, V</i>	24.798	0.011	2.862	0.014	isolated; close to edge of image
PC	5	16:23:55.56	-26:32:32.1	<i>V</i>	23.615	0.007	1.690	0.014	isolated
PC	132	16:23:55.10	-26:32:04.2	<i>I, V</i>	25.969	0.033	3.295	0.036	isolated; next to saturated star
WF2	21	16:23:53.41	-26:31:29.1	<i>V</i>	24.041	0.034	2.468	0.036	next to saturated star; very near to edge of image
WF2	24	16:23:53.56	-26:31:29.8	<i>V</i>	24.952	0.021	2.806	0.026	next to saturated star
WF2	73	16:23:53.87	-26:31:24.1	<i>V</i>	24.040	0.021	2.552	0.027	next to saturated star
WF2	120	16:23:54.35	-26:31:24.6	<i>I</i>	26.096	0.029	2.418	0.036	next to saturated star
WF2	277	16:23:56.44	-26:31:31.1	<i>I, V</i>	24.097	0.036	2.839	0.046	next to saturated star
WF2	395	16:23:59.37	-26:31:57.2	<i>V</i>	24.923	0.033	2.218	0.035	close to edge of image
WF2	511	16:24:00.26	-26:31:48.3	<i>V</i>	25.243	0.014	3.173	0.018	near to saturated star; close to edge of image
WF2	515	16:23:58.25	-26:31:10.3	<i>I</i>	25.377	0.029	3.046	0.036	isolated; appears to be two overlapping PSFs
WF2	585	16:24:00.68	-26:31:37.1	<i>V</i>	21.197	0.024	1.368	0.031	isolated; close to edge of image
WF2	661	16:23:56.63	-26:32:21.7	<i>V</i>	25.530	0.027	3.006	0.029	close to bright star
WF3	58	16:23:59.89	-26:33:21.0	<i>V</i>	20.853	0.011	1.865	0.012	isolated
WF3	392	16:24:02.42	-26:32:59.9	<i>I, V</i>	24.117	0.036	0.565	0.039	isolated; very near to edge of image
WF3	554	16:24:00.53	-26:31:49.8	<i>V</i>	21.152	0.015	1.203	0.020	isolated
WF3	611	16:24:01.13	-26:31:49.2	<i>V</i>	22.406	0.025	1.349	0.026	isolated; close to edge of image
WF3	613	16:24:01.34	-26:31:52.8	<i>V</i>	25.322	0.023	3.122	0.025	isolated; close to edge of image
WF3	619	16:24:01.02	-26:31:45.7	<i>I</i>	19.978	0.053	1.411	0.059	isolated; close to edge of image
WF4	11	16:23:53.74	-26:32:53.0	<i>V</i>	24.614	0.033	2.711	0.036	near another star - PSFs may be overlapping
WF4	53	16:23:56.65	-26:32:32.6	<i>I, V</i>	24.965	0.021	2.781	0.022	isolated; very near to edge of image
WF4	55	16:23:56.58	-26:32:33.7	<i>V</i>	21.333	0.005	1.960	0.006	isolated
WF4	58	16:23:52.32	-26:33:13.8	<i>V</i>	21.965	0.024	2.070	0.027	next to saturated star
WF4	63	16:23:56.58	-26:32:34.8	<i>I, V</i>	22.648	0.009	1.880	0.010	isolated
WF4	190	16:23:53.79	-26:33:16.9	<i>V</i>	24.564	0.020	2.638	0.023	next to saturated star
WF4	345	16:23:53.61	-26:33:42.4	<i>V</i>	24.964	0.022	1.436	0.023	isolated; very near to edge of image
WF4	427	16:23:56.32	-26:33:32.0	<i>I, V</i>	25.599	0.016	2.735	0.020	near another star - PSFs may be overlapping
WF4	550	16:23:56.72	-26:33:48.3	<i>I, V</i>	24.235	0.030	0.580	0.032	isolated; near to saturated star
WF4	551	16:23:59.03	-26:33:26.9	<i>I, V</i>	24.550	0.013	2.742	0.016	isolated; near to

Table 1—Continued

Chip	ID	RA ^a	Dec ^a	Filters ^b	<i>V</i>	σ_V	<i>V</i> – <i>I</i>	σ_{V-I}	Comments
WF4	555	16:23:59.14	-26:33:26.1	<i>I</i> , <i>V</i>	24.877	0.024	2.794	0.028	saturated star
WF4	563	16:23:59.19	-26:33:26.5	<i>I</i> , <i>V</i>	22.291	0.031	1.431	0.035	isolated
WF4	579	16:23:55.60	-26:34:02.3	<i>V</i>	22.006	0.020	2.118	0.021	isolated; near to saturated star
WF4	581	16:23:55.30	-26:34:05.6	<i>V</i>	23.336	0.022	2.413	0.029	isolated; close to edge of image

^aAll coordinates are in J2000.

^bFilter in which star was identified as an outlier.

Table 2. M4 main sequence and white dwarf sequence outliers chosen as candidates for variability search.

Chip	ID	RA	Dec	V	σ_V	$V - I$	σ_{V-I}	Comments
PC	1	16:23:56.26	-26:32:27.0	22.349	0.024	0.831	0.042	isolated; very near to edge of image
PC	97	16:23:54.33	-26:32:20.6	22.639	0.009	0.706	0.015	isolated
WF2	404	16:23:56.79	-26:31:07.1	24.480	0.027	2.882	0.029	isolated
WF3	78	16:23:58.95	-26:32:58.1	25.262	0.023	3.554	0.027	isolated; near to saturated star
WF3	532	16:24:02.37	-26:32:29.9	24.014	0.023	2.786	0.027	isolated; next to diffraction spike of saturated star
WF3	625	16:24:02.30	-26:32:08.4	27.190	0.027	2.821	0.029	isolated; next to diffraction spike of saturated star; very near to edge of image
WF4	284	16:23:54.03	-26:33:29.6	23.985	0.018	2.044	0.019	isolated; near two saturated stars
WF4	327	16:23:57.94	-26:32:59.9	23.409	0.021	2.572	0.025	isolated
WF4	335	16:23:56.22	-26:33:16.9	22.937	0.016	1.884	0.018	isolated
WF4	473	16:23:54.87	-26:33:53.3	24.443	0.010	3.007	0.016	next to diffraction spike of saturated star
WF4	519	16:23:57.81	-26:33:31.4	22.926	0.013	2.153	0.018	isolated; near to diffraction spike of saturated star

Table 3. ZZ Ceti variable star candidates.

Chip	ID	RA	Dec	X	Y	<i>V</i>	σ_V	$V - I$	σ_{V-I}
WF2	340	16:23:58.88	-26:32:00.0	70.567	456.524	24.515	0.025	0.649	0.028
WF4	286	16:23:54.13	-26:33:29.0	388.078	660.529	24.621	0.026	0.700	0.028
WF4	550	16:23:56.72	-26:33:48.3	749.814	482.751	24.235	0.030	0.580	0.032

Table 4. Artificial star test results using Algol-type light curves.^a

Magnitude	Input	Output	% Recovered			
			P	$\frac{1}{2}P$	$\frac{3}{2}P$	other
<i>I</i> -band data						
17.0	74	72	96.0	0.0	0.0	4.0
18.0	74	68	91.9	0.0	0.0	8.1
19.0	74	73	98.6	0.0	0.0	1.4
20.0	74	71	95.9	0.0	0.0	0.0
21.0	74	70	94.6	0.0	0.0	5.4
22.0	74	68	91.9	0.0	0.0	8.1
23.0	74	69	90.6	1.3	0.0	8.1
24.0	74	65	36.5	4.0	0.0	59.5
25.0	74	3	1.4	1.4	0.0	97.2
<i>V</i> -band data						
19.0	74	72	0.0	0.0	96.0	4.0
20.0	74	68	0.0	0.0	91.9	8.1
21.0	74	73	2.7	1.4	93.2	2.7
22.0	74	71	9.5	8.2	73.0	9.3
23.0	74	70	18.9	12.2	40.6	28.3
24.0	74	68	23.0	9.5	24.4	43.1
25.0	74	69	22.9	14.8	8.1	54.2
26.0	74	65	8.1	4.0	1.3	86.6
27.0	74	3	0.0	0.0	0.0	100.0

^aPrimary eclipse depth is ≈ 0.3 mag.

Table 5. Artificial star test results using W UMa-type light curves.^a

Magnitude	Input	Output	% Recovered			
			P	$\frac{1}{2}P$	$\frac{3}{2}P$	other
<i>I</i> -band data						
17.0	74	71	94.6	0.0	0.0	5.4
18.0	74	68	91.9	0.0	0.0	8.1
19.0	74	73	97.3	1.4	0.0	1.3
20.0	74	72	95.9	1.4	0.0	2.7
21.0	74	71	89.2	6.7	0.0	4.1
22.0	74	69	77.0	16.2	0.0	6.8
23.0	74	68	60.8	29.8	0.0	9.4
24.0	74	64	18.9	45.9	0.0	35.2
25.0	74	2	0.0	2.7	0.0	97.3
<i>V</i> -band data						
19.0	74	71	0.0	95.9	0.0	4.1
20.0	74	68	1.4	90.5	0.0	8.1
21.0	74	73	2.7	96.0	0.0	1.3
22.0	74	72	5.4	91.8	0.0	2.8
23.0	74	71	12.2	81.1	0.0	6.7
24.0	74	69	28.3	62.2	0.0	9.5
25.0	74	68	32.4	56.8	0.0	10.8
26.0	74	64	8.1	23.0	1.4	67.5
27.0	74	2	0.0	2.7	0.0	97.3

^aPrimary eclipse depth is ≈ 0.2 mag.